ALPHA - BETA TRANSITION IN QUARTZ

A THESIS SUBMITTED TO
THE GRADUATE SCHOOL OF NATURAL AND APPLIED SCIENCES
OF
MIDDLE EAST TECHNICAL UNIVERSITY

BY

MUSTAFA CEM LİDER

IN PARTIAL FULFILLMENT OF THE REQUIREMENTS
FOR
THE DEGREE OF MASTER OF SCIENCE
IN
PHYSICS

SEPTEMBER 2011

Approval of the thesis:

ALPHA - BETA TRANSITION IN QUARTZ

submitted by **MUSTAFA CEM LİDER** in partial fulfillment of the requirements for the degree of **Master of Science in Physics Department, Middle East Technical University** by,

Prof. Dr. Canan Özgen _____
Dean, Graduate School of **Natural and Applied Sciences**

Prof. Dr. Sinan Bilikmen _____
Head of Department, **Physics**

Prof. Dr. Hamit Yurtseven _____
Supervisor, **Physics Dept., METU**

Examining Committee Members:

Assoc. Prof. Dr. Barış Akaoğlu
Physical Engineering Dept., Ankara University _____

Prof. Dr. Hamit Yurtseven
Physics Dept., METU _____

Assoc. Prof. Dr. Enver Bulur
Physics Dept., METU _____

Assoc. Prof. Dr. Akif Esendemir
Physics Dept., METU _____

Assist. Prof. Dr. Alpan Bek
Physics Dept., METU _____

Date: _____

I hereby declare that all information in this document has been obtained and presented in accordance with academic rules and ethical conduct. I also declare that, as required by these rules and conduct, I have fully cited and referenced all material and results that are not original to this work.

Name, Last Name: MUSTAFA CEM LİDER

Signature :

ABSTRACT

ALPHA - BETA TRANSITION IN QUARTZ

Lider, Mustafa Cem
M.Sc., Department of Physics
Supervisor : Prof. Dr. Hamit Yurtseven

September 2011, 49 pages

Alpha-Beta transition in quartz is studied using the Raman scattering. The Raman frequencies of some lattice modes are analyzed at various temperatures close to the alpha beta transition in quartz. For this analysis, the experimental data from the literature is used and the soft mode behavior of those Raman phonons is investigated . On the basis of the predictions of some models, the temperature dependencies for the Raman frequencies of the lattice modes which move towards zero (soft mode) and their bandwidths close to the transition temperature T_c are explained for the alpha-beta transition in quartz. In addition, by using the experimental volume data from literature, calculation of the temperature dependence of the Raman frequencies through the Grüneisen parameter have been studied near the phase transition.

Keywords: $\alpha-\beta$ Transition, Raman Frequency, Bandwidth, Soft Mode, Grüneisen Parameter, Quartz.

ÖZ

KUARTZIN ALFA BETA GEÇİŞİ

Lider, Mustafa Cem
Yüksek Lisans, Fizik Bölümü
Tez Yöneticisi : Prof. Dr. Hamit Yurtseven

Eylül 2011, 49 sayfa

Kuartzın alfa - beta geçişi Raman saçılması kullanılarak çalışılmıştır. Bazı örgü kiplerinin Raman frekanslarının analizi kuartzın alfa beta geçişi yakınındaki çeşitli sıcaklıklarda yapılmıştır. Bu analiz için, literatürden deneysel veri kullanılmış ve bu Raman fononlarının yumuşak kip davranışı araştırılmıştır. Bazı modellerin tahminlerine dayanarak, sıfıra doğru giden (yumuşak kip) örgü kiplerinin Raman frekanslarının sıcaklığa bağımlılığı ve geçiş sıcaklığı T_c yakınındaki bant genişlikleri kuartzın alfa beta geçişi için açıklanmıştır. Ayrıca, yine literatürden deneysel hacim verileri kullanılarak faz geçişi yakınlarında Grüneisen parametresi aracılığıyla sıcaklığa bağlı Raman frekanslarının hesabı yapılmıştır.

Anahtar Kelimeler: Alfa-Beta Geçişi, Raman Frekansı, Bant Genişliği, Yumuşak Kip, Grüneisen Parametresi, Kuartz.

To my parents

ACKNOWLEDGMENTS

I would like to express my sincere feelings to everyone who contributes me to study in this thesis. Foremost, I gratefully acknowledge Prof. Dr. Hamit Yurtseven for his insight, guidance and continuous support throughout the study. Honestly, I emphasize that this thesis could not have been possible without his unique effort.

I would like to thank also H. Yeliz Öztürk for her help on personal matters and for kindly support. Moreover, my special thanks goes to Kamil Çınar for his help about PC software during the writing.

TABLE OF CONTENTS

LIST OF TABLES

TABLES

LIST OF FIGURES

FIGURES

CHAPTER 1

INTRODUCTION

There have been quite a lot of experimental studies of structural phase transition since the early of 1940s. In this field of study, various spectroscopic techniques have been used to analyze physical and chemical properties of materials, including Raman scattering, neutron scattering, infrared (IR) reflectivity, x-ray, electron paramagnetic resonance (EPR), nuclear quadrapole resonance (NQR) and ultrasonic analyses [1]. Of the techniques, Raman spectroscopy has been widely become standard method in vibrational spectroscopy. As an inelastic light scattering by molecular vibrations, it was first developed by Raman and consequently he was awarded the Nobel prize in 1930 [2].

Raman spectroscopy method is used to analyze the vibrational modes of material having unique process and selection rules. Unlike IR spectroscopy which is used to study of the asymmetric vibrations of polar groups, Raman spectroscopy is the best at symmetric vibrations of non polar groups [2].

Raman scattering , as an inelastic scattering arises from change of the frequency of incident light after passing through a sample. The incoming light with a higher energy than the vibrational energy interacts with the molecule. The shift of frequency between incident and scattered lights gives the information of vibrational energy states of relevant molecule. This significant shift called Raman shift is given by the expression below

$$\Delta\omega = \left(\frac{1}{\lambda_0} - \frac{1}{\lambda_1}\right) \tag{1.1}$$

where $\Delta\omega$ is the Raman shift in the unit of cm^{-1}, λ_0 and λ_1 are the excitation wavelength and the Raman spectrum wavelength, respectively, in the units of cm.

The Raman spectrum has been notably used to study the lattice dynamics of crystals. Especially, temperature dependence of lattice vibrations near the phase transition temperature is a widely attractive issue. For this purpose, the Raman spectroscopy is of vital importance to explain the phase transition and critical phenomena.

In this thesis, the phase transition in quartz has been investigated by using Raman scattering. The data from the literature has been used to analyze the quartz crystal near the transition temperature. The Raman spectrum of crystalline quartz (SiO_2) has been investigated using the experimental data [3] for the lattice modes between the temperatures of 77 and 888 K. It is shown here that the Raman shifts of the 147 cm^{-1} and 207 cm^{-1} modes play a significant role while approaching from α phase to the β phase of quartz. This phenomena has been explained by the soft mode theory.

$\alpha-\beta$ transition in quartz has been the subject of various studies given in literature. Between the α and β phases, an intermediate phase (incommensurate) has been observed in a temperature range of 1.3 ^oC by the measurements of the heat capacity and the thermal expansion [4]. A sharp peak in C_p has been observed at the incommensurate IC-β transition, whereas at the α-IC transition the C_p peak becomes rounded around the transition temperature [5]. In the incommensurate phase as a thermodynamically stable phase determined by x-ray diffraction topography [6], there are six equivalent modulated waves excited within the c-plane [7] [8].

The thermodynamic nature of the $\alpha-\beta$ transition in quartz has been determined by an anomaly in heat capacity by means of differential scanning calorimetry (DSC) [4] and, also in thermal dilatation and dielectric constant [9]. A second order transition which occurs above the first-order transition from α to β, has been proposed based on the observations of thermal expansion and elastic compliance [10]. A first order (discontinuous) or second order (continuous) nature of the $\alpha-\beta$ transition in quartz has also been discussed in an earlier study [11].

Some spectroscopic studies have given evidence of a first and second order kind that occurs near the $\alpha-\beta$ transition in this crystal. In particular, the Raman spectra have shown that the lattice vibration of the 207 cm^{-1} mode is associated with the $\alpha-\beta$ transition [3]. This is supported by the temperature dependence of the Raman linewidth and shift of optical lattice vibrations in quartz [12]. Also, the opalescence in a quartz crystal that has been observed near the $\alpha-\beta$ transition [13] describes the critical behavior of the order parameter related to the intensity in the spectrum. It has been argued that the critical opalescence that originates from

the divergence of the fluctuations of the order parameter, can possibly affect on the Raman scattering of the soft mode [13].

In regard to the order parameter due to the orientation of SiO_4 tetrahedra, which can take two opposite values in the α phase corresponding to Dauphine twins (it is zero in the β phase), it has been suggested [11] that Landau theory (mean field theory) can be employed. According to the domain model for the β phase, the atoms occupy different $\alpha-$domains which gives dynamic disorder in the high-symmetry β phase at high temperatures. On cooling, they occupy the positions corresponding to one domain in the low-symmetry α phase [14]. According to the classical soft-mode picture, vibrations of the atoms around their mean positions change the symmetry at T_c as the temperature decreases from the β phase to the α phase in quartz and displacive mode acts as the classical soft mode [14]. It has been pointed out previously [15] that both models do not explain satisfactorily the structure of quartz and that low-energy high-amplitude vibrations can contribute to the disorder in the β phase. Regarding the low temperature α phase, there appear four symmetric Raman-active modes of species A_1 and eight doubly degenerate Raman active modes of species E, as reported previously [3]. Only one of those A_1 modes, which corresponds to the displacements of the atoms at the transition [16] is the 207 cm^{-1} mode associated with the $\alpha - \beta$ transition, as stated above. It has been observed experimentally that the 207 cm^{-1} Raman mode exhibits strong variation with the temperature [3] [17]. Experimental data [3] gives that this Raman mode does not disappear in the β phase, whereas the 147 cm^{-1} Raman mode which shows anomalous behavior disappears completely at the $\alpha - \beta$ transition ($T_c = 846K$). The 147 cm^{-1} Raman mode of species A_1 has been considered as a soft mode [3] since its frequency goes to zero as the T_c is approached.

The $\alpha - \beta$ transition in quartz was considered as the $\lambda - point$ transition at 573 ^oC and the Pippard relations were applied to this crystal many years ago [18]. An anomalous behavior of the heat capacity near the $\alpha - \beta$ transition has been detected experimentally [4] [19]. An observed anomaly in thermal dilatation and dielectric constant has also been reported [9]. The $\alpha - \beta$ transition in quartz is considered as a first order since there is a thermal hysteresis of 1 to 2 ^oC between heating and cooling, as obtained from the heat capacity measurements [4]. However, the adiabatic measurements show that the C_p diverges with $\Delta H = 0$ [20] which suggests that the $\alpha-\beta$ transition is of a second order. In the presence of the intermediate phase (incommensurate IC) between the α and β phases, it has been pointed out that the transition upon cooling from β to IC is a second order with a small discontinuity and that the transition

from IC to α is a first order [4] [10].

The $\alpha-\beta$ transition in quartz can be explained by two neighboring structures due to the atomic positions with a rotation of the tetrahedric SiO_4 angle φ (2-order axis), which causes the change of the symmetry between the α and β phases (3 to 6 order) as pointed out previously [21]. In an earlier study [14], temperature dependence of the fourth power of the average SiO_4 tetrahedral tilt angle δ has been taken as the order parameter of the $\alpha-\beta$ transition. It has also been pointed out that there are phonon modes propagating, which are not interacting with the SiO_4 tetrahedra so that the tetrahedra move as rigid bodies with rotations of the Si-O-Si linkages [14]. As the temperature increases from the α phase to β phase, the frequency of those phonon modes decrease, which is an indication of disorder and thus the soft mode is excited. Among the phonon modes which are associated with the $\alpha-\beta$ phase transition in quartz, as observed experimentally [17] [3] the 207 cm^{-1} Raman mode exhibits strong variation with temperature. The Raman frequency of this mode exists above T_c, whereas the other lattice mode of the 147 cm^{-1} shows anomalous behavior and its Raman frequency goes to zero at $T = T_c$. This is a soft mode behavior [22] so that the 147 cm^{-1} Raman mode plays an important role in the mechanism of the $\alpha-\beta$ transition in quartz.

The $\alpha-\beta$ transition in this crystal has been investigated by the shift in T_c, which can be associated with the thermal expansion of granite at high pressure [23]. The transition temperature T_c has also been associated with a supercooling in an X-ray work [19]. Some other experimental studies regarding the structure of $\beta-quartz$ and the existence of the $\alpha-\beta$ transition have been given in literature. $\alpha-\beta$ transition in MXO_4 quartz like materials in regard to structure deformations has been studied experimentally [24]. As given in a previous study [25], β-quartz crystallizes in a hexagonal symmetry and its chemical bond is ionic-covalent. There are three SiO_2 molecules in the unit cell and the unit cell parameters at 848 K are $a = 4.9965$ Å and $c = 5.4546$ Å [25]. Structural changes in the $\alpha-\beta$ transition in quartz have also been studied in an earlier work [26] [27].

The Raman frequencies can be predicted from the volume data through the mode Grüneisen parameter for the $\alpha-\beta$ transition in quartz. By using the variation of the crystal volume with temperature and the value of the mode Grüneisen parameter, the frequencies of the Raman modes can be calculated as a function of temperature for the $\alpha-\beta$ transition in quartz.

In this study, we analyze the experimental data [3] for the temperature dependencies of the

147 cm^{-1} and 207 cm^{-1} Raman modes using a power-law formula. We associate variation of the Raman frequency of those modes with the order parameter for the $\alpha - \beta$ transition in quartz. By using the temperature dependence of the 147 cm^{-1} and 207 cm^{-1} Raman modes, we then calculate the damping constant (Raman bandwidths) at various temperatures using the soft mode-hard mode and the energy fluctuation models. The activation energies of the two lattice modes (147 cm^{-1} and 207 cm^{-1}) are also calculated for the $\alpha - \beta$ transition in quartz. In addition, we calculate the temperature dependence of the Raman frequencies for the lattice mode of 207 cm^{-1} for the $\alpha-\beta$ transition in quartz. For this prediction of the Raman frequencies of the 207 cm^{-1} mode, we use the volume data [14] and the observed Raman data for this mode [3] to determine the value of the mode Grüneisen parameter.

The arrangement of the thesis is as follows:
In chapter 2, phase transitions and types, transition from the α phase to the β phase in quartz, order parameter, Landau theory, soft mode the models for the damping constant and also the Grüneisen parameter are included. In chapter 3, the analyses of Raman bandwidth for both the 147 cm^{-1} and 207 cm^{-1} modes and calculation of the Grüneisen parameter are given. As a final chapter (chapter 4), the results of the calculations are given and comparison with the theoretical values is discussed.

CHAPTER 2

THEORY

2.1 Phase Transition

Phase transition is defined by transforming from one phase to another for a stable structure. A very common example is water. By heating the water from liquid phase to gaseous phase we can observe a simple phase transition. At 100 ^{o}C water molecules begin to leave the liquid surface and steam is emitted. This process between different phases is very sudden. At the boiling point the liquid water becomes thermodynamically unstable and gaseous water becomes stable. In order to increase the temperature of material, the heat should be applied. The heat capacity is determined how much heat is needed since applying heat to the material increases its entropy [28]. Hence, the relation of heat capacities can be given as

$$C_\alpha = T\left(\frac{\partial S}{\partial T}\right)_\alpha \tag{2.1}$$

where α is the corresponding constant (*eg.* V, P, etc). Considering the two phases which are in thermodynamic equilibrium at a critical temperature T_c, one needs to add some extra heat in order to transform from one phase to another which is called as the latent heat given by

$$L = \Delta Q = T_c(S_2 - S_1) \tag{2.2}$$

where S_1 and S_2 are the entropies of the first phase and second phase, respectively. According to Equations 2.1 and 2.2, we can say that there exists a jump in the heat capacity C_α as a function of temperature. In Figure 2.1 the temperature dependence of entropy is shown in the existence of latent heat in liquid-gas transition where T_b represents the boiling point.

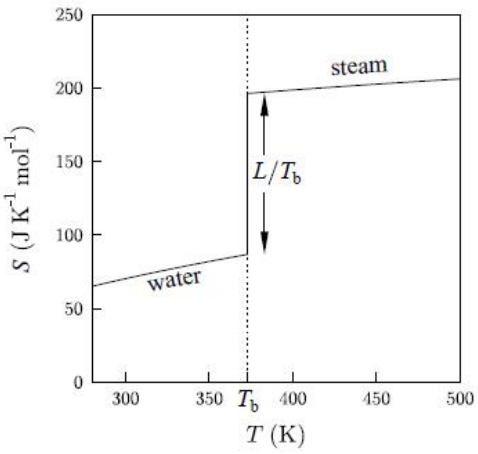

Figure 2.1: Temperature dependence of entropy of H_2O [28].

A phase diagram of water is shown in Figure 2.2 in which three phases of solid, liquid and gaseous are given, coexisting with the phase boundaries.

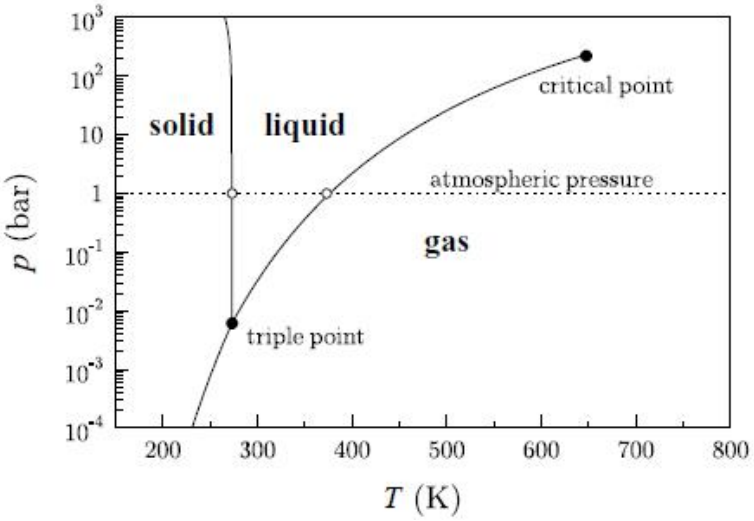

Figure 2.2: Phase diagram of H_2O [28].

Solid, liquid and gaseous phases coexist at the triple point. There exist a very steep boundary between the solid and liquid phases while approaching from the liquid to solid phase, a large change occurs in entropy and small change in volume. This boundary of phase does not terminate and continues indefinitely. On the other hand, the boundary between gas and liquid terminates at the critical point. The latent heat of changing from solid to gas (sublimation) is

the sum of the latent heat of melting and the latent heat of vaporisation at temperatures close to the triple point [28].

Most of substance expand in consequence of melting, so the gradient of solid-liquid line is positive. Since water shrinks slightly when it melts, the gradient of solid-liquid line is negative as shown in Figure 2.2 due to the hydrogen bonding that ice crystal lattice has an open structure.

The stability at a temperature T is given by the minimum of Helmholtz free energy,

$$F = U - TS \tag{2.3}$$

where U is the internal energy and S is the entropy. This relation for the different phases is the same at transition temperature T_c as

$$F_1(T_c) = F_2(T_c) \tag{2.4}$$

where T_c is below the melting point [29]. So as to decide the type of phase, it is appropriate to consider the Gibbs function g which depends on the temperature and pressure. The Gibbs function is defined as [30]

$$dg = -S\,dT + V dP \tag{2.5}$$

where S and V are entropy and volume, respectively. Hence

$$\left(\frac{\partial g}{\partial T}\right)_P = -S \quad and \quad \left(\frac{\partial g}{\partial P}\right)_T = V\ . \tag{2.6}$$

The classification of phase transition is defined by Ehrenfest as a first order, second order, third order and also fourth order. However, only the first two types of transition are mainly of interest.

According to Ehrenfest, the order of a transition can be described using the Gibbs function. It is simply defined that the transition is the first order provided that g is continuous but its

derivatives $(\frac{\partial g}{\partial T})_P$ and $(\frac{\partial g}{\partial P})_T$, that is, -$S$ and V respectively, are discontinuous with the existence of latent heat. On the other hand, if there is no latent heat and no volume change the Gibbs function is continuous but the second derivatives, namely, compressibility, specific heat and expansion coefficient are discontinuous. Such a type of transition is said to be the second order [30]. In Figure 2.3, the temperature dependence of corresponding parameters (gibbs function, volume, specific heat) in the first order transition are shown.

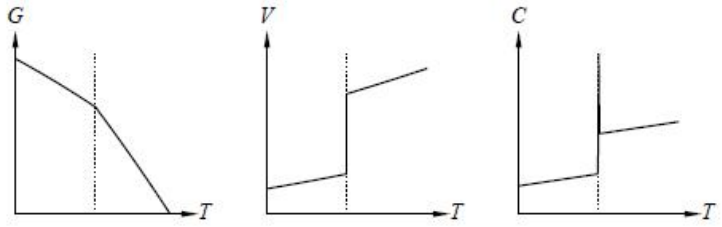

Figure 2.3: First order transition [28].

In figure 2.4, the behavior of corresponding parameters (gibbs function, volume, specific heat) that depend on temperature in the second order transition are shown. An example of this phase transition type is superconductivity transition on the order-disorder transition in β brass.

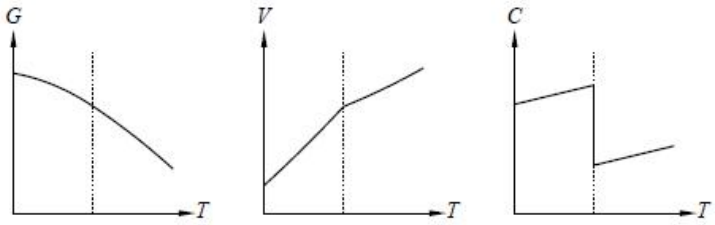

Figure 2.4: Second order transition [28].

A modern approach to classification of phase transitions differs from including latent heat or not. One is first order transition as in first order phase transition of Ehrenfest, the other is continuous phase transition including second, third and fourth order transitions of Ehrenfest.

Another classification of phase transition includes the symmetry breaking. An example of this broken symmetry is illustrated in Figure 2.5 as below the transition temperature (T_c) and above this temperature. In this example, atoms in a solid and in a liquid are compared.

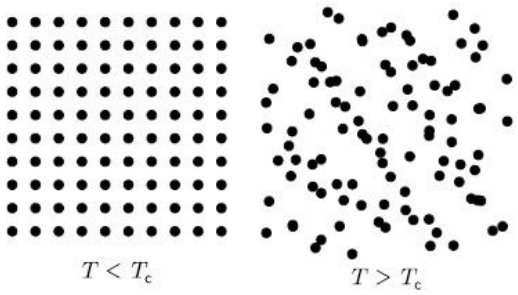

Figure 2.5: The liquid ($T > T_c$)-solid ($T < T_c$) phase transition [28].

In a liquid phase, the contraction of the system is weak but has a high degree of symmetry. In the solid phase, however, this symmetry is broken. Firstly, one may see a surprising picture in Figure 2.5 as if solid looks more symmetrical than liquid. But this situation is in fact different. It is necessary to note that any point in a liquid is the same as any other on average. Atoms do not line up just a direction or axes, rather the system possess rotational and translational symmetry. On the other hand, solid is of some residual symmetry and it is invariant under four-fold rotations. To change symmetry gradually is impossible and a certain symmetry is either present or not. Therefore, phase transition is sharp and there is a particular distinction between disordered and ordered phase [28].

2.1.1 Polarization

Polarization is the macroscopic quantity of dielectric materials. Since the tendency of polarization (polarizability) for diverse substance is different, it can be said that the dielectric property is a characteristic property represented by dielectric constant ϵ. A dielectric material can interact with an electric field seeing that electric dipoles line up to this field. Number of dipole moments per unit volume is defined as polarization which is represented by the polarization vector

$$\vec{P} = (\epsilon - \epsilon_0)\vec{E} = \chi_e \epsilon_0 \vec{E} \tag{2.7}$$

where ϵ_0 is the electric permittivity of space, ϵ is the electric permittivity of the medium and χ_e is the susceptibility. The average dipole moment ($\vec{\mu_{av}}$) of particle is related with local

electric field $\vec{E}_{loc}$ as

$$\vec{\mu_{av}} = \alpha \vec{E_{loc}} \tag{2.8}$$

where α is the polarizability which measures the electric susceptibility of the particle. With the relation between polarization and N elementary dipole moments of particles $\vec{\mu_{av}}$ as

$$\vec{P} = N\vec{\mu_{av}} \tag{2.9}$$

the expression of polarization can be reduced as follows

$$\vec{P} = N\alpha \vec{E_{loc}} \ . \tag{2.10}$$

Here $\vec{E_{loc}}$ is different from $\vec{E}$ owing to the polarization of surrounding dielectric medium. Based on these parameters, the polarization can be investigated by the change of temperature, frequency and applied field. The polarizability (α) can be divided into four contribution parts as electronic, ionic, orientational and interfacial in the form of

$$\alpha = \alpha_e + \alpha_i + \alpha_d + \alpha_s \ . \tag{2.11}$$

In electronic polarization, there exist positive atomic nuclei surrounded by negative electron clouds. By applying an external electric field,electrons are slightly displaced and consequently induced dipole moments are formed. In ionic polarization, an external electric field gives rise to change the equilibrium positions of net charges which have opposite polarity. The asymmetric distribution of these distinct charges cause the permanent dipole moments even in the absence of external electric field. However, these permanent dipoles experience a torque due to the external electric field. Then we can say that orientational polarization arises from the orientation of dipole moments towards the applied field direction. These three contributions of polarization arise from the charges which are bounded in atoms locally. On the other hand, in the interfacial polarization (space charge polarization), charge carriers can migrate some amount of distance in dielectric substance. During this displacement process the

charge carriers can be trapped on interfaces or in the material. All these kinds of polarization are illustrated in Figure 2.6 [31].

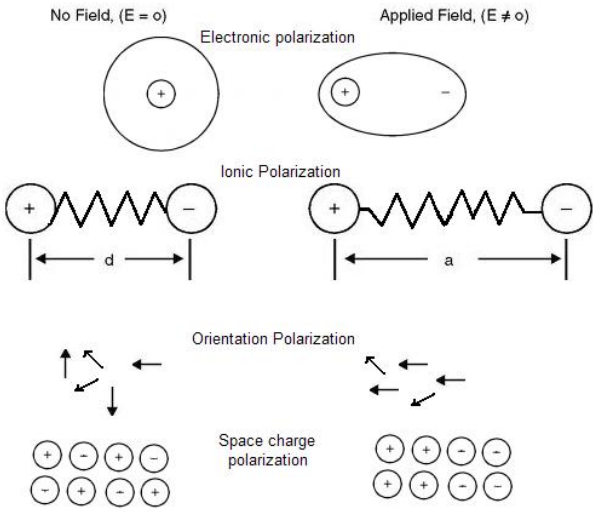

Figure 2.6: Polarization mechanisms [31].

2.1.2 Transition Types of Ferroelectric Crystals

As far as structural transition is concerned, the ferroelectric transition has been extensively studied in which the spontaneous polarization plays fundamental role in crystals. In such crystals extraordinary temperature dependence of dielectric constant is of widely interest. Therefore, this property has been discussed in order to explain piezoelectric effect, pyroelectric effect and electro optical effects [29].

It has been accepted that ferroelectric crystals can be classified as order-disorder or displacive. This type of crystals is marked due to their own type of transition as either displacive or order-disorder. Both types of transitions are the transformation from one phase (*e.g.* ferroelectric phase) to another (*e.g.* paraelectric phase) at the transition temperature or Curie temperature T_c with a slightly reversible temperature change near the T_c.

In a displacive transition, the oscillations of atomic displacements in a paraelectric phase change from the region about a non-polar to a polar region. Moreover, in an order-disorder transition, the oscillations of the displacements in a paraelectric phase, however, change from the region of some double-well or multi-well configuration to about an ordered subset of these

wells [29].

2.1.3 Landau Theory of Phase Transitions

The concept of thermodynamic properties of structural phase transition takes back to the investigation of Landau (1937). According to him, the transition can be explained in terms of an order parameter η of which breaks the symmetry of the paraelectric phase at Curie temperature (T_c). While η is non-zero below the T_c, it vanishes above the T_c. Therefore, η is such a significant parameter that plays crucial role on the atomic configuration from the less symmetrical phase to the more symmetrical paraelectric phase [32].

"In order-disorder transition η measures the amount of long range ordering of permanent dipoles. In displacive transitions, on the other hand, η measures the degree of displacement of certain ions or ionic groups, *i.e.*, the long range ordering of induced dipoles."[32]

By making a perfect analogy to the ferromagnetism, one can say that while the order parameter is magnetization in ferromagnetic crystals, it is polarization in ferroelectric crystals. The hysteresis property of P depending on electric field E is shown in Figure 2.7 [33].

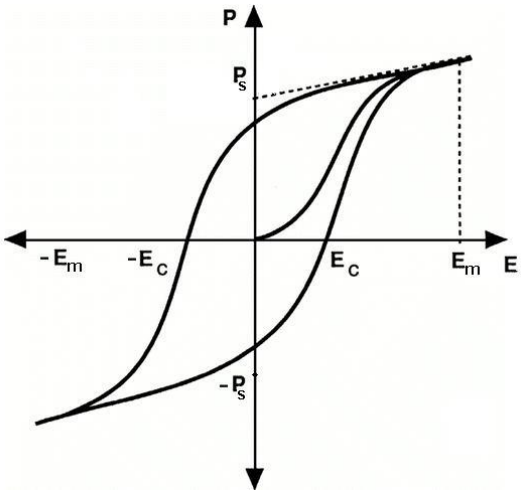

Figure 2.7: Hysteresis loop for the polarization [33].

Here, P_s is the spontaneous polarization which is defined by the bounded surface charge density on the relevant sample owing to the relative atomic displacements in a phase transition, E_m and E_c are maximum applied electric field and coercive field, respectively.

According to Landau, we can define ϕ as the thermodynamic potential depending on T and η, in addition, the potential can be selected as Helmholtz free energy given in Equation 2.3. By saying η_0 as the equilibrium value of the order parameter in the absence of external field, ϕ ought to be minimum for the corresponding temperature for unstable states [32]

$$\left(\frac{\partial\phi}{\partial\eta}\right)_{\eta_0} = 0, \qquad \left(\frac{\partial^2\phi}{\partial\eta^2}\right)_{\eta_0} > 0\ . \tag{2.12}$$

The above relations are used to determine the stability of diverse phases. In reference to Landau, this potential should be expanded in powers of η as [32]

$$\phi = \phi_0 + \frac{1}{2}a\eta^2 + \frac{1}{4}b\eta^4 + \frac{1}{6}c\eta^6 + ... \tag{2.13}$$

where ϕ_0 is the thermodynamic potential at which $\eta = 0$, a and b are temperature dependent functions. The order parameter η is the spontaneous polarization P for the ferroelectric phase transition. In Equation 2.13, the coefficient of η^4, b is of such a significant role that it determines the transition type as a first order, second order transition or tricritical. If $b > 0$, it is the second order, $b < 0$ it is the first order and when $b = 0$, it is tricritical phase transition. The Figures 2.8 and 2.9 represent the temperature dependence of the polarization for the first order and second order transitions, respectively [32].

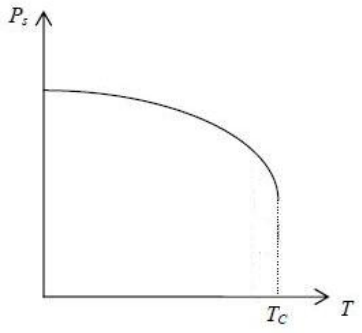

Figure 2.8: Temperature dependence of polarization for the first order transition [32].

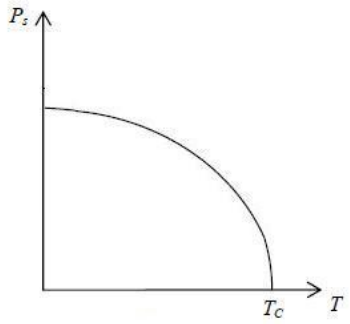

Figure 2.9: Temperature dependence of polarization for the second order transition [32].

Therefore, Equation 2.13 becomes

$$\phi = \phi_0 + \frac{1}{2}\phi_1 P^2 + \frac{1}{4}\phi_2 P^4 + \frac{1}{6}\phi_3 P^6 + ... \tag{2.14}$$

Applying the first condition of relation in Equation 2.12

$$\left(\frac{\partial \phi}{\partial P}\right)_{P_0} = 0 \tag{2.15}$$

one finds

$$(\phi_1 + \phi_2 P_0^2) P_0 = 0 \ . \tag{2.16}$$

The above equation has two solutions, one is $P_0 = 0$ and the other is $P_0 \neq 0$ by neglecting higher powers than P^4 for simplicity. It is useful to explain the even powers of order parameter related to continuous phase transition, whereas the odd ones are omitted corresponding to discontinuous phase transition. Here, the even powers should be selected for the ferroelectric and ferromagnetic crystals.

As a further step, applying the latter relation in Equation 2.12 we can write straightforwardly

$$\left(\frac{\partial^2 \phi}{\partial P^2}\right) > 0. \tag{2.17}$$

In the existence of an external electric field E and defining the second derivative of free energy

density with respect to the polarization is the reciprocal of isothermal susceptibility χ_T^{-1} [32]. Hence,

$$\left(\frac{\partial \phi}{\partial P}\right) = E \tag{2.18}$$

$$\left(\frac{\partial^2 \phi}{\partial P^2}\right)_{P_0} = \frac{\partial E}{\partial P} = \frac{1}{\chi_T} > 0 \ . \tag{2.19}$$

It is straightforward to see the polarization from the Equation 2.16.

$$P_0 = \sqrt{\frac{-\phi_1}{\phi_2}} \ . \tag{2.20}$$

For the first solution $P_0 = 0$ is valid for $T > T_c$, namely, the paraelectric phase. As far as the second solution $P_0 \neq 0$ is concerned, we can say that a non-zero polarization exist even if there is no external field. In order to seek the behavior in the neighborhood of the transition temperature T_c, it is appropriate to expand ϕ in Taylor series by assuming [32]

$$\phi_1 = a'(T - T_c) \tag{2.21}$$

where a' is constant. Then Equation 2.20 becomes

$$P_0 = \left(\frac{a'}{\phi_2}\right)^{\frac{1}{2}} (T - T_c)^{\frac{1}{2}} \tag{2.22}$$

where T is below the transition temperature T_c. And finally, this relation can be reduced as

$$P_0 \ \alpha \ (T - T_c)^{\beta} \qquad T < T_c \tag{2.23}$$

where β is the critical exponent for the polarization and its value $\beta = \frac{1}{2}$ [32].

2.1.4 Soft Mode and Displacive Transition

In the study of Raman spectroscopy, the optical phonons of the sample analyzed has been investigated since the optical phonons are interacting with the incident beam in the Brillouin

zone of sample in Raman scattering. So, these phonon frequencies as transverse (TO) and longitudinal (LO) are the basis of measurement. With the same wave vector, longitudinal optical phonon frequencies are higher than the frequencies of the transverse optical. Since TO phonon frequency vanishes at any point within the Brillouin zone, this type of phonons can be investigated rather than LO phonons. A typical dispersion relation is shown in figure 2.10. Precisely, we can say that the phonon frequency is of important role in the displacive phase transition.

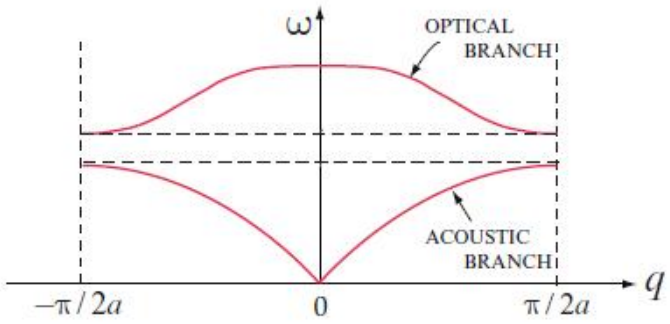

Figure 2.10: Dispersion relation [34].

As the measured property of phase transition, the symmetry breaking occurs while passing from one phase to another. In ferroelectric crystals as an order parameter, the spontaneous polarization P, is zero at higher temperatures (higher symmetry), whereas it is non-zero at low temperatures, (low symmetry).

For the continuous transitions, namely, the second order transition below the critical temperature T_c, we can define a "normal mode" of which frequency is zero $\tilde{\nu}(\vec{q} = 0) = 0$ that rebuilds the lost symmetry [32].

Let us think a phonon frequency with a wave vector $\vec{q}$ by using anharmonic interaction approach. It can be defined as

$$\tilde{\nu} = \nu_0^2 + \alpha T \tag{2.24}$$

where the constant α is positive. Here, ν_0 is the harmonic frequency of phonon. The anharmonic addition increases up to the fact that this restoring frequency $\tilde{\nu}$ comes to zero [22].

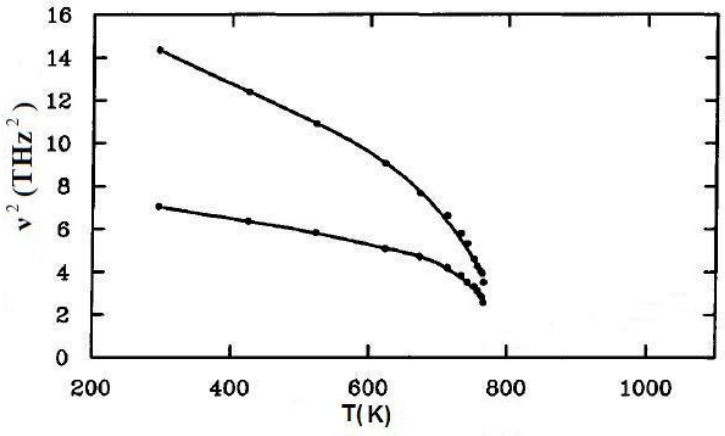

Figure 2.11: Temperature dependence of soft mode [22].

In the low temperature (less symmetric) phase, the frequency of mode decreases down to zero by heating to the critical temperature T_c. At T_c the crystal presents an unstable state and the phase transition occurs from the low symmetric phase to high symmetric phase. The behavior of the lowering frequency while approaching to the transition temperature is defined as "soft mode" [22]. In Figure 2.11, the behaviour of the soft mode is shown for the $PbTiO_3$ obtained by Scott and Burns in 1970 using Raman spectroscopy [22]. Quartz also shows the behaviour of soft mode with $\vec{q} = 0$, although it is not ferroelectric. It has a lack of inversion symmetry for both low and high temperature phases [22].

2.2 Quartz

Quartz, SiO_2, is the most abundant crystal on earth. One silicone and four oxygen atoms are bounding and each Si is shearing the O atoms with the neighboring Si, consisting of SiO_2 [35]. As the polymorphs, there are six types of quartz in terms of stability at different temperatures.

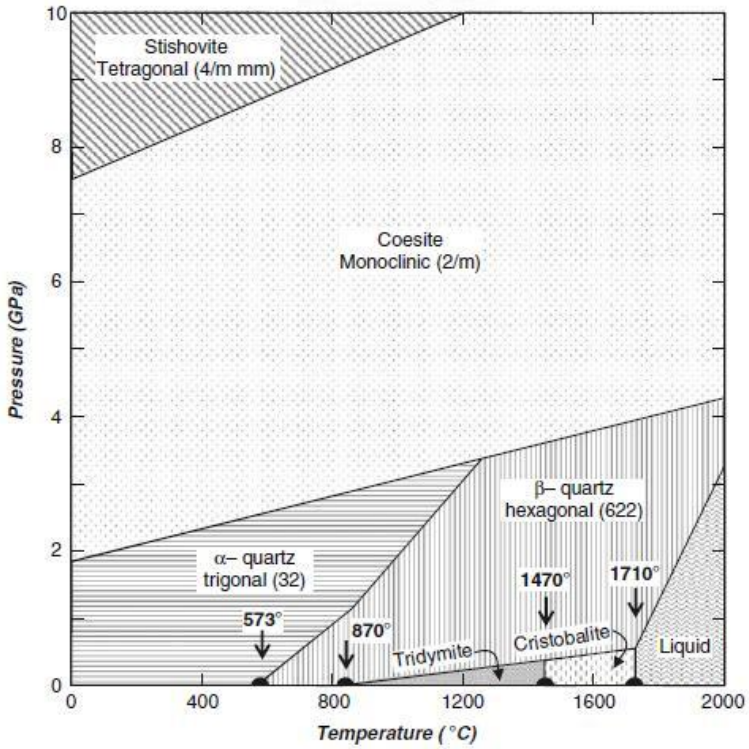

Figure 2.12: Polymorphs of SiO_2 [36].

They are $\alpha - quartz$, $\beta - quartz$, tridymite, cristobalite, coesite and stishovite. With the pressure and temperature dependence of quartz types is shown in figure 2.12 [36]. Since our investigation is on alpha quartz and beta quartz, we do not focus on the others.

Quartz refers to α quartz or low quartz that exists below the 573.3^oC ($\sim$ $840K$) with the point group of D_3 and trigonal structure. It has the enantiomorphistic property that exhibits the chiral structure as the space groups of $P3_121(D_3^4)$ and $P3_121(D_3^6)$. At room temperature, the lattice constants of unit cell a_0 and c_0 are 0.4918 nm and 0.5404 nm, respectively. The bonding of Si-O consists of approximately 0.4 ionic and 0.6 covalent with the $\sim$ 4.85 eV bonding energy[36].

By heating, α quartz transforms to β quartz or high quartz above the transition temperature T_c, moving Si atoms at an amount of 0.03 nm. The trigonal shape changes to hexagonal with the point groups of D_6 and space groups $P6_222(D_6^4)$ and $P6_422(D_6^5)$. At about 873 K the lattice constants of unit cell are $a_0 = 0.501\ nm$ and $c_0 = 0.547\ nm$ [36]. Furthermore, $\beta - phase$

has higher symmetry than the $\alpha - phase$ and their structures are shown in Figure 2.13 by comparing only the Si atoms of each phase [27].

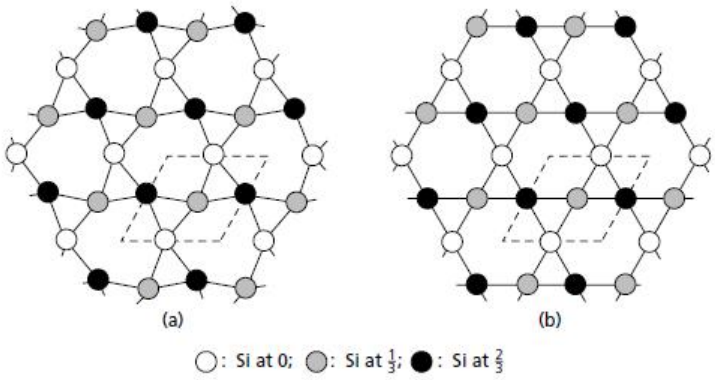

Figure 2.13: (a) $\alpha - quartz$ and (b) $\beta - quartz$ [27].

The structure of quartz was first investigated by Bragg and Gibbs in 1925. Ever since, numerous studies have been developed to analyze the structure of quartz, using x-ray and neutron scattering [37]. In 1940, Raman and Nedungadi have first analyzed the structure phase transition of quartz using Raman scattering. They observed the soft mode behavior while approaching the transition temperature T_c, from the $\alpha - phase$ to the $\beta - phase$.

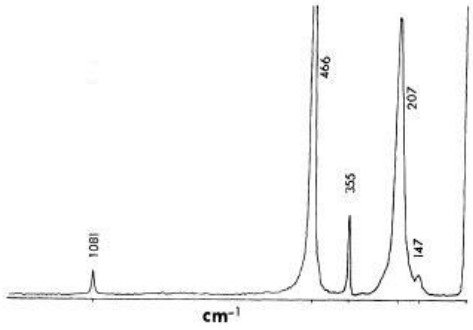

Figure 2.14: Raman spectrum of $\alpha - quartz$ with species A_1 at room temperature [3]

Then after a decade, Cochran and Anderson claimed that the vibrational normal modes present instability which give rise to the phase transition in some ferroelectric crystals. According to them, the mode frequency exhibits decreasing down to zero, as approaching T_c with the

relation of $\nu^2 \sim \mid T - T_c \mid$ [38]. Considering the Landau's theory, Ginzburg suggested that the soft mode behavior is the main rule of second order transition [39].

By the group theory, the types and the numbers of modes in crystals can be theoretically calculated. In this respect, for $\alpha - quartz$ in the low temperature there exists four Raman active and eight double degeneracy modes, species A and E, respectively. The modes having A_1 are determined as 1081, 466, 356 and 207 cm^{-1} [16]. Of these four modes, the three of them transform to species of B_1 Raman-inactive during the phase transition. Therefore, only one mode of species A_1 (Raman-active) survives in the $\beta - phase$.

In the study of Shapiro *et al.* [3], between the temperatures 77 and 888 K, quartz crystal has been experimentally investigated. However, in addition to the usual expectation of the modes for the $\alpha - quartz$, an unexpected mode of 147 cm^{-1} was observed and it is shown in Figure 2.14. This mode was found to obey soft mode accompanying with the 207 cm^{-1} mode. These two modes of quartz present a high variation with the temperature change. While the 147 cm^{-1} mode frequency exists only in $\alpha - phase$, not in the $\beta - phase$, 207 cm^{-1} mode is present in both phases. So that, it is reasonable to say based on the experimental result that there is only one A_1 mode in the $\beta - phase$ and there are five modes in the $\alpha - phase$. The experimental outcome of both phases is shown in Figure 2.15. Since the E modes present a little change with the varying temperature, they have not been considered in details.

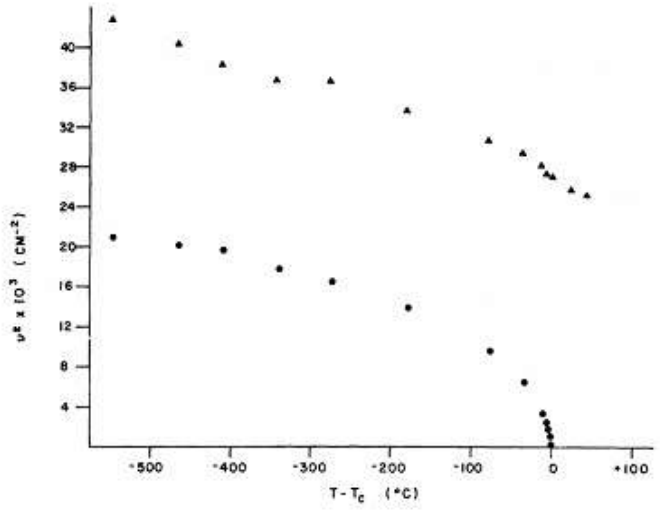

Figure 2.15: Soft mode behavior of the 207 cm^{-1} and 147 cm^{-1} mode frequencies [3]

In this figure, the triangles are for the 207 cm^{-1} and circles for the 147 cm^{-1} modes. Behavior of the temperature dependence of these two mode frequencies can be explained by the soft mode theory with the $\nu^2 \sim \mid T - T_c \mid^{\gamma}$ where the excepted value of critical exponent γ as $0.4 < \gamma < 0.5$ [3].

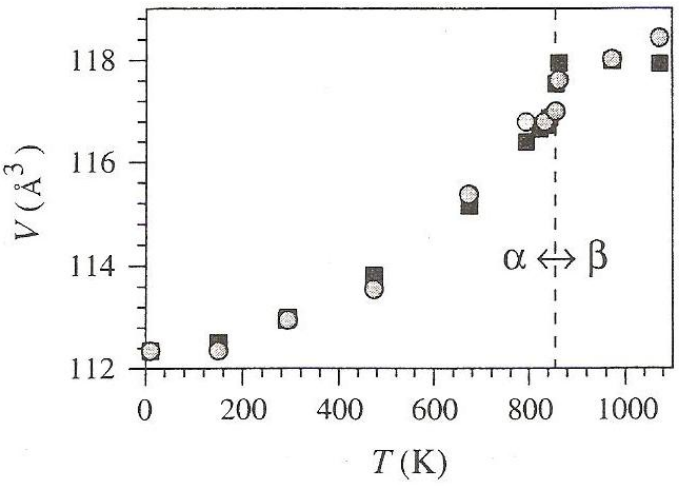

Figure 2.16: The temperature dependence of volume expansion in quartz [14]

One of the other analysis of the $\alpha - \beta$ phase transition on quartz has been studied by Tucker *et al.* [37]. The temperature dependence of unit cell volume approaching from the $\alpha - phase$ to the $\beta - phase$ with a range of 20 to 1073 K, has been analyzed by using neutron scattering. In this study, the increasing volume of the unit cell, as shown in Figure 2.16, has been observed and the average structure of quartz (squares) with the neutron diffraction data (circles) was comparably considered. The expansion of unit cell volume was explained in details merely for silicon and for oxygen in view of transforming the structure trigonal to hexagonal system [37].

2.3 Raman Bandwidth

The anharmonic effects in crystals lead to observe thermal expansion, temperature dependent phonon frequencies, elastic constants and also bandwidths of phonon frequencies. Of these effects, two of them play significant role on phonons, one is the deviation from the harmonic interaction and the other is damping of phonon frequencies, observed as bandwidth and broadening of the Raman spectrum line. One example of the latter behavior is shown in Figure 2.17

for KNO_3 analyzed by Harris in 1992. Linewidth or damping constant can be defined as "the inverse of life time of an excited state" [22].

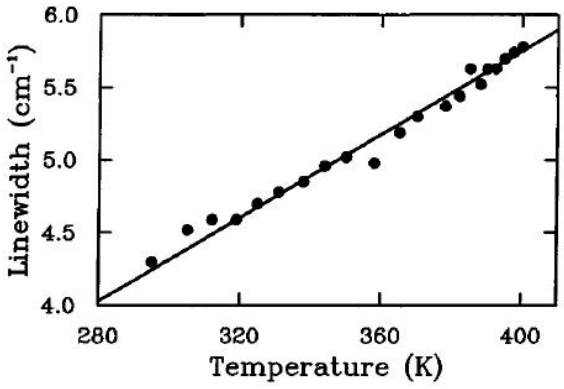

Figure 2.17: Temperature dependence of bandwidth of a $\vec{q} = 0$ mode for KNO_3 [22].

A compact expression of damping constant has been derived by Laulicht and Lucknar in 1977 [40] beginning with the study of Yamada *et al.* [41] on Ising spin-phonon coupled system and more general treatment of Matsushita [42] in 1976 as follows:

$$\Gamma = \Gamma_0 + A(1 - P^2)\, ln\Big(\frac{T_c}{T - T_c(1 - P^2)}\Big) \tag{2.25}$$

where P and Γ_0 are the order parameter and damping constant of background respectively, with constant A. In addition to Equation 2.25, a further expression has been developed by Laulicht [43] in 1978 as

$$\Gamma = \Gamma_0 + A' \left(\frac{(1 - P^2)T}{T - T_c(1 - P^2)}\right) \tag{2.26}$$

with a constant A'. Here, the order parameter is temperature dependent and given by Matsushita [42] in the molecular field theory as,

$$1 - 2exp\Big[-\frac{2T_c}{T}\Big] \ , \ T << T_c$$

$$P = \ \Big[3\Big(1 - \frac{T}{T_c}\Big)\Big]^{\frac{1}{2}} \ , \ 0 < T_c - T < T_c \tag{2.27}$$

$$0 \quad , \ T_c < T$$

According to this relation, P the order parameter does not exist above the transition temperature. So that, the ν^2 can be related to P linearly by

$$\nu^2 = a + bP \tag{2.28}$$

where a and b are constants.

Regarding the soft mode-hard mode model, the critical behavior of the damping constant can be described according to a power-law formula

$$\Gamma = A[T/(T_c - T)]^{2\beta} \tag{2.29}$$

where β is the critical exponent for the order parameter and A is the amplitude. This relation can be written in the logarithmic form as

$$ln\Gamma = lnA + 2\beta \ ln[T/(T_c - T)] \tag{2.30}$$

During the phase transitions ions can be differently oriented by gaining an amount of activation energy E_a. The relation with the damping constant is given by Huber *et al.* [44] as

$$\Gamma = \alpha + \frac{\beta}{T} \ exp[-E_a/k_BT] \tag{2.31}$$

where k_B is the Boltzmann constant, α and β are also constants related with the relaxation of vibration and reorientation of relaxation, respectively. Very close to transition temperature these coefficients can be ignored, hence using this approximation the Equation 2.31 reduces to

$$ln\Gamma = \left(\frac{-E_a}{k_B T}\right). \tag{2.32}$$

2.4 Grüneisen Parameter

To study the thermal expansion during the phase transition we have to use anharmonic approximation to explore the unit cell volume dependence of phonon frequencies. In order to obtain so called Grüneisen relation, it is useful to begin with the heat capacity. A conservation relation of heat capacity between constant pressure (C_p) and constant volume (C_v) with the temperature is the following:

$$C_p - C_v = \frac{TV\alpha^2}{\kappa_T} \tag{2.33}$$

where κ_T and α are the isothermal compressibility and the expansion coefficient, respectively

$$\kappa_T = -\frac{1}{V}\left(\frac{\partial V}{\partial P}\right)_T \tag{2.34}$$

$$\alpha = \frac{1}{V}\left(\frac{\partial V}{\partial T}\right)_P = \kappa_T\left(\frac{\partial P}{\partial T}\right)_V. \tag{2.35}$$

The derivative of Helmholtz free energy with respect to the volume, that is P, gives

$$P = -\left(\frac{\partial F}{\partial V}\right)_T = -\frac{\partial \phi}{\partial V} - \frac{1}{2}\sum_{\vec{q},\nu}\hbar\frac{\partial\omega(\vec{q},\nu)}{\partial V} - \sum_{\vec{q},\nu} n(\omega,T)\hbar\frac{\partial\omega(\vec{q},\nu)}{\partial V} \tag{2.36}$$

substituting into the Equation 2.4 yields

$$\alpha = -\kappa_T \sum_{\vec{q},\nu}\hbar\frac{\partial\omega(\vec{q},\nu)}{\partial V}\frac{\partial n(\omega,T)}{\partial T} \tag{2.37}$$

where n is the phonon number and ν stands for the labeled mode. So, the heat capacity with the contribution of each mode is expressed as

$$\tilde{C}_{\vec{q},\nu} = \hbar\omega(\vec{q},\nu)\frac{\partial n(\omega,T)}{\partial T} \tag{2.38}$$

and also the Grüneisen parameter of mode can be defined as

$$\gamma_{\vec{q},\nu} = -\frac{V}{\omega(\vec{q},\nu)}\frac{\partial\omega(\vec{q},\nu)}{\partial V} = -\frac{\partial\Big(ln\omega(\vec{q},\nu)\Big)}{\partial(lnV)} \tag{2.39}$$

with the mean Grüneisen parameter

$$\gamma = \sum_{\vec{q},\nu}\gamma_{\vec{q},\nu}\frac{\tilde{C}_{\vec{q},\nu}}{C_v} \tag{2.40}$$

In Equation 2.39, the minus sign contributes a positive effect on γ. And it is appropriate to say that whereas the frequency is decreasing, the volume of unit cell is increasing due to the weakness of inter-atomic forces [22]. For a constant pressure in case of the isobaric state, changing the unit cell volume by the temperature can be related to the variation of the frequency with temperature, defined as the isobaric mode Grüneisen parameter,

$$\gamma_p = -\frac{1}{\alpha}\frac{1}{\nu}\Big(\frac{\partial\nu}{\partial T}\Big)_p \, . \tag{2.41}$$

By means of this equation, the Raman frequency varying with the temperature can be expressed as

$$\nu_p(T) = \Delta\nu + \nu_1 \; exp[-\gamma_p ln(V_p(T)/V_1)] \tag{2.42}$$

where V_1 and ν_1 are the volume and frequency, respectively, at T=0 K and $\Delta\nu$ is the frequency shift. The temperature dependence of volume V_p(T) and the frequency $\nu_p(T)$ can be expressed by a quadratic formula

$$V_p = a_0 + a_1T + a_2T^2 \tag{2.43}$$

and

$$\nu_p = b_0 + b_1T + b_2T^2 \, . \tag{2.44}$$

CHAPTER 3

CALCULATIONS

3.1 Analysis of the Two Raman Frequencies of 147 cm^{-1} and 207 cm^{-1} Modes of Quartz

In the study of Shapiro *et al.* [3], for the α-β phase transition in quartz, two Raman frequency modes of 147 cm^{-1} and 207 cm^{-1} show significant changes with the varying temperature as an anharmonic effect. This behavior has been observed within the temperatures 77 K to 888 K, for the α-phase to β. From the curve of these two modes in Figure 2.15 by approaching to critical temperature T_c, a soft mode like picture can clearly be seen. We took the data for both modes to analyze the soft mode behavior obeying the power-law formula $\nu^2 = k \mid T - T_c \mid^{\beta}$ and obtained the values of the critical exponent β. We plotted for the 147 cm^{-1} mode in Figure 3.1 and the 207 cm^{-1} mode in Figure 3.2 by separating the fitted curves into two. In order to obtain the values of the critical exponent β as in Equation 2.23, each mode was analyzed with the corresponding temperature intervals.

Table 3.1: Values of the critical exponent for the Raman frequencies of the 147 cm^{-1} and 207 cm^{-1} modes and the amplitude according to power-law formula

Raman mode (cm^{-1})	β	**k**	**Temperature interval (K)**
147	0.5	897.8	$4.3 <\mid T - T_c \mid< 546.3$
147	1.2	298.8	$0.5 <\mid T - T_c \mid< 4.3$
207	0.2	10938.0	$179.3 <\mid T - T_c \mid< 543.3$
207	0.04	24343.0	$1.4 <\mid T - T_c \mid< 179.3$

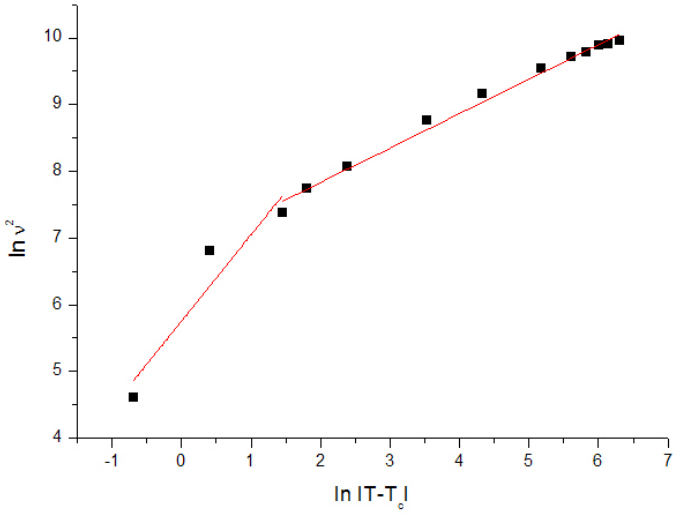

Figure 3.1: Temperature dependence of the 147 cm^{-1} Raman mode frequency as approaching to the critical temperature T_c.

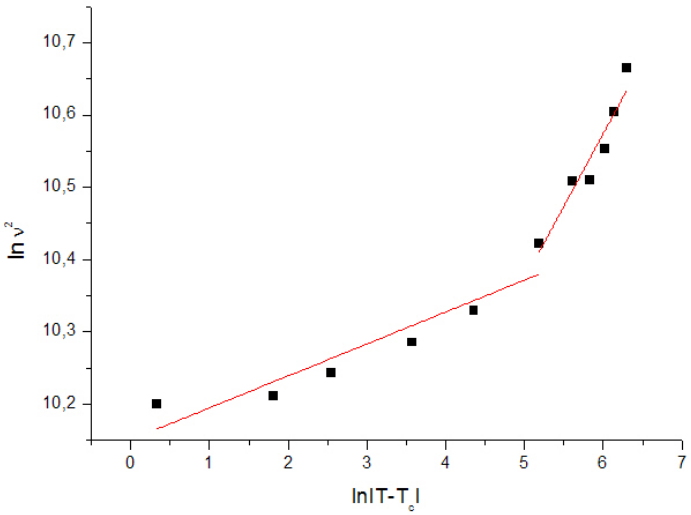

Figure 3.2: Temperature dependence of the 207 cm^{-1} Raman mode frequency as approaching to the critical temperature T_c.

3.2 Calculation of the Damping Constant for the 147 cm^{-1} and 207 cm^{-1} Raman Modes

According to the bandwidth relations in Equations 2.25 and 2.26, we calculated the damping constant denoted as Γ_1 and Γ_2, respectively. For the 147 cm^{-1} mode, Γ values have a coupled behavior, so that we plotted them separately as two linear fits. However, damping constant of the 207 cm^{-1} mode required to be fitted a cubic function.

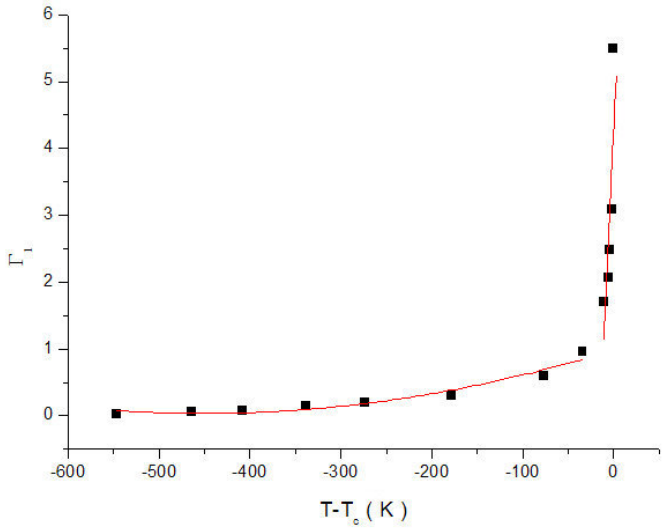

Figure 3.3: Temperature dependence of the damping constant according to Equation 2.25 for the 147 cm^{-1} mode.

In Figure 3.3 the diverging part of the fitted line was redrawn in Figure 3.4 by using a power low formula given in Equation 2.29 to find the critical exponent β close to the transition temperature. After doing this, values of the critical exponent β corresponding to the damping constants Γ_1 and Γ_2 are listed in Table 3.2.

Table 3.2: Values of the critical exponent β and the amplitude A for 147 cm^{-1} near the T_c.

Bandwidth	β	A (cm^{-1})	**Temperature interval (K)**
Γ_1	0.18	0.34	$0.5 < \mid T - T_c \mid < 10.8$
Γ_2	0.28	0.18	$0.5 < \mid T - T_c \mid < 10.8$

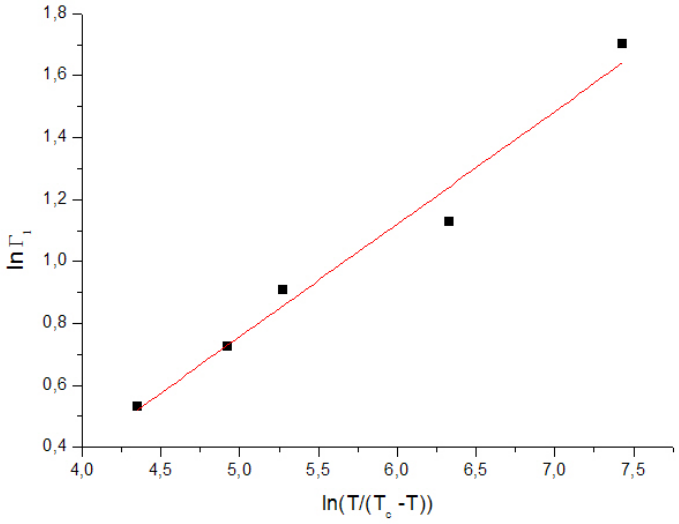

Figure 3.4: The diverging part of the damping constant near the T_c.

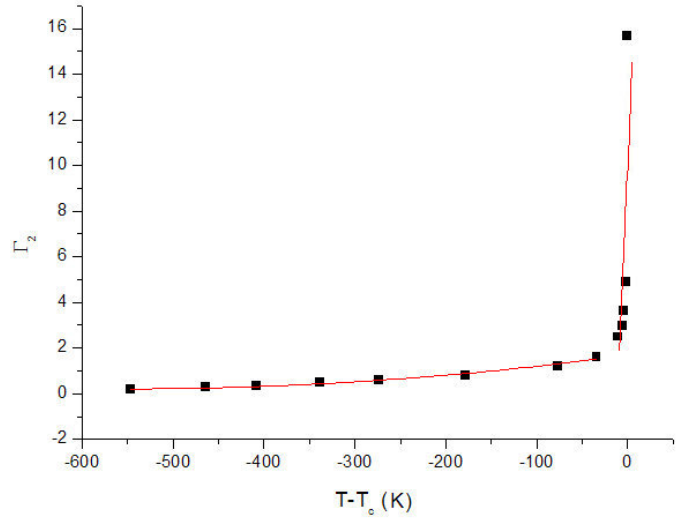

Figure 3.5: Temperature dependence of the damping constant according to Equation 2.26 for the 147 cm^{-1} mode

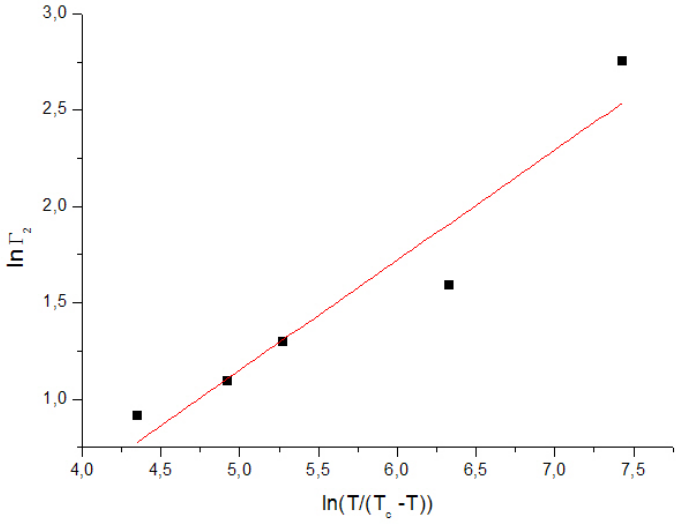

Figure 3.6: The diverging part of the damping constant near the T_c

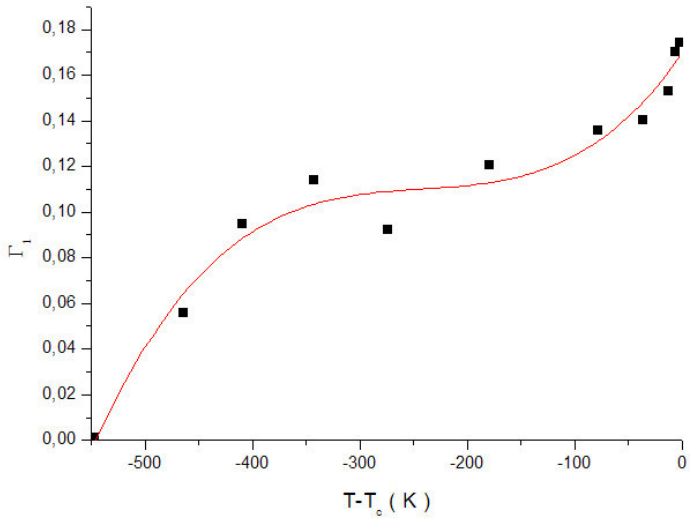

Figure 3.7: Temperature dependence of the damping constant fitted with a cubic function for the 207 cm^{-1} mode according to Equation 2.25.

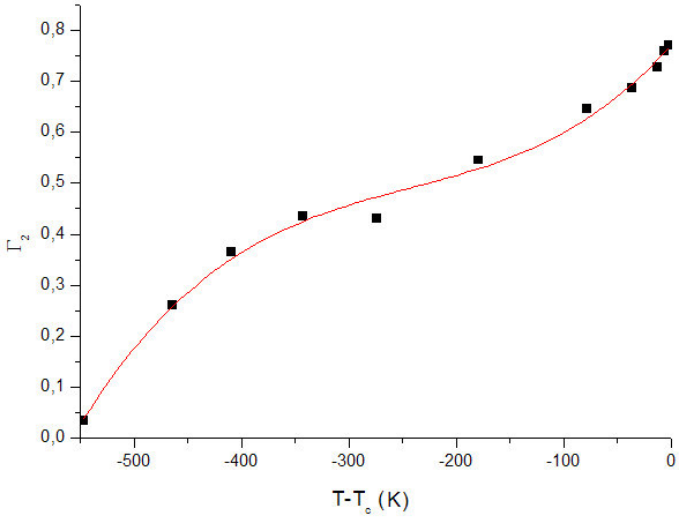

Figure 3.8: Temperature dependence of damping constant fitted with a cubic function for the 207 cm^{-1} mode according to Equation 2.26

3.3 Calculations of the Order Parameter and Raman Frequencies of the 147 cm^{-1} and 207 cm^{-1} Modes

In this study, the order parameter (polarization) was calculated using the second relation of Equation 2.27. By making use of the ν^2 *vs* P graphs , each mode frequency was calculated and compared with the observed ones.

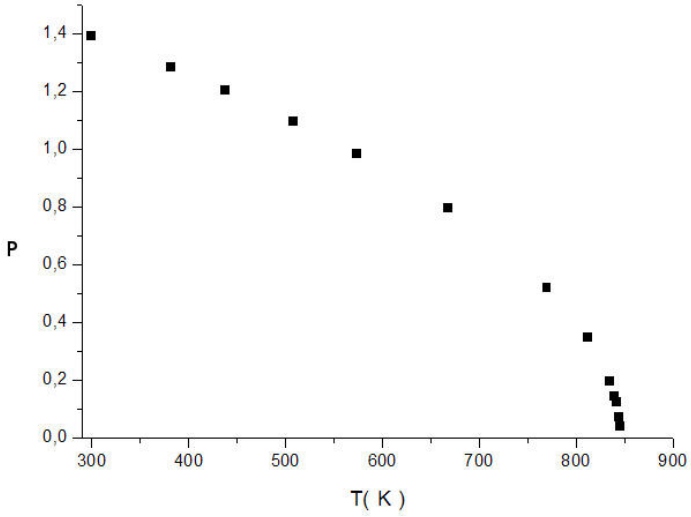

Figure 3.9: Temperature dependence of the order parameter (polarization P)

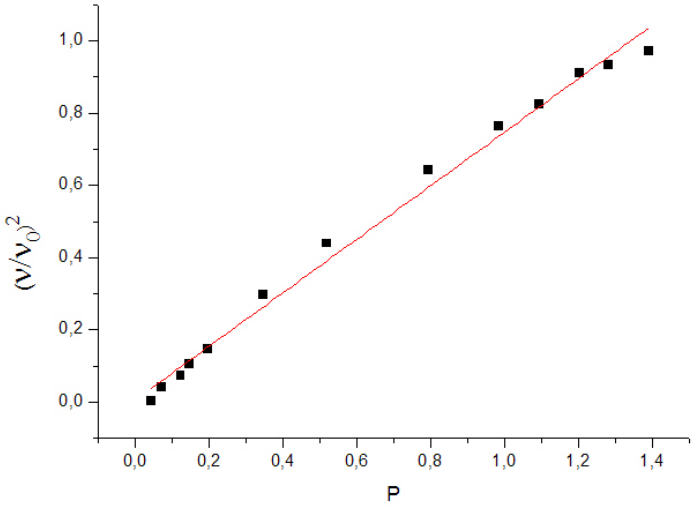

Figure 3.10: ν^2 *against* P relation for the 147 cm^{-1} Raman mode

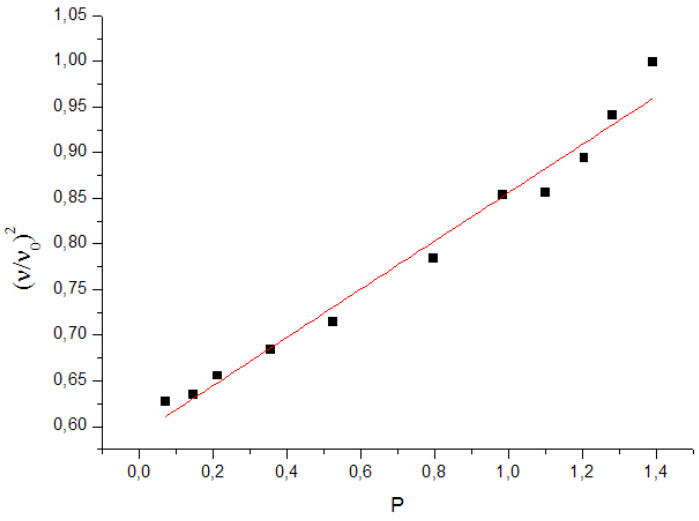

Figure 3.11: v^2 *against* P relation for the 207 cm^{-1} Raman mode

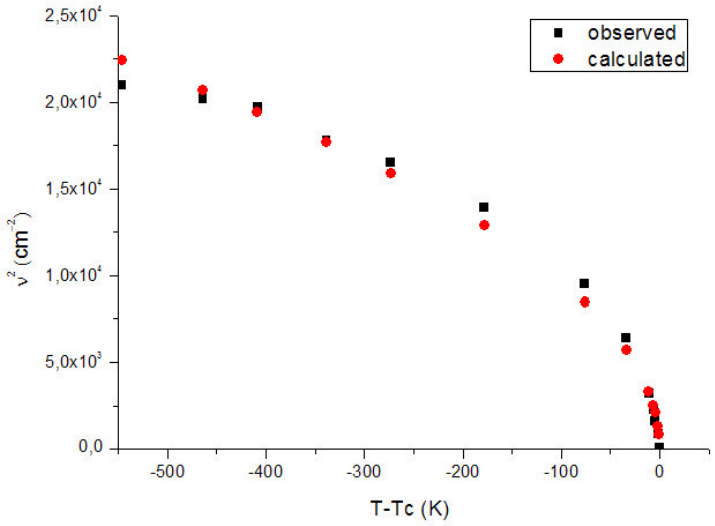

Figure 3.12: Calculated and observed frequencies for the 147 cm^{-1} Raman mode

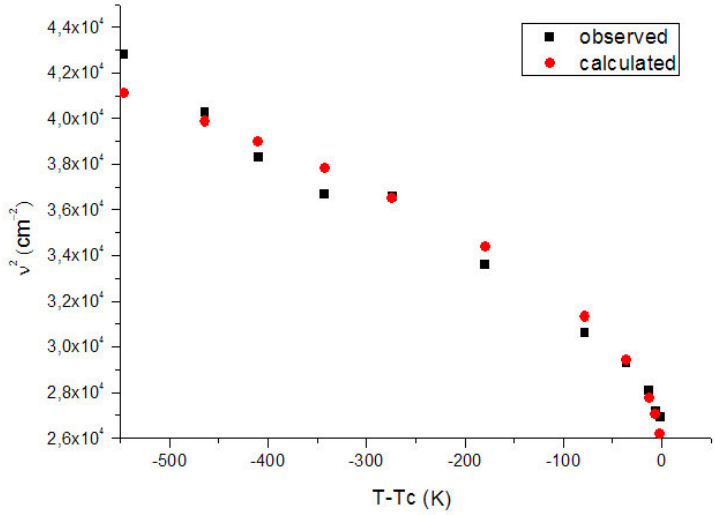

Figure 3.13: Calculated and observed frequencies for the 207 cm^{-1} Raman mode

3.4 Calculation of the Activation Energy for the 147 cm^{-1} and 207 cm^{-1} Raman Modes

According to Equation 2.32, the activation energy E_a using the Raman bandwidths Γ_1 and Γ_2 was calculated and relevant temperature intervals are listed.

Table 3.3: Calculation of the activation energies for the Raman modes indicated

Raman mode (cm^{-1})	Γ	E_a (eV)	**Temperature interval (K)**
147	Γ_1	1.32	$769.8 < T < 845.6$
147	Γ_1	0.11	$299.8 < T < 769.8$
147	Γ_2	1.22	$769.8 < T < 845.6$
147	Γ_2	0.07	$299.8 < T < 769.8$
207	Γ_1	0.005	$382.1 < T < 844.7$
207	Γ_2	0.005	$382.1 < T < 844.7$

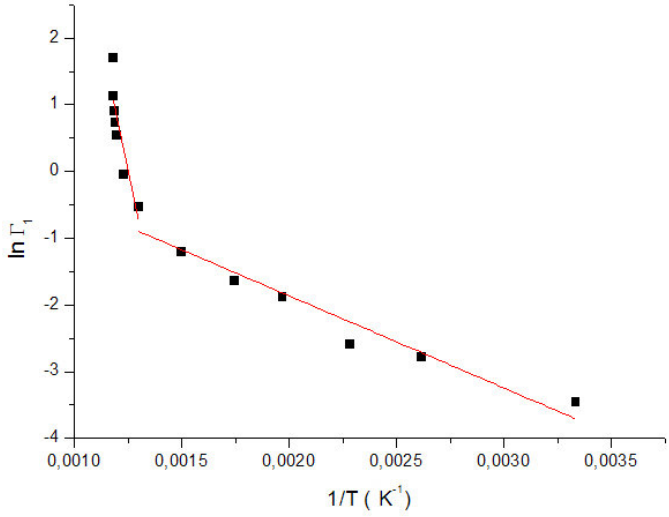

Figure 3.14: The damping constant (Γ_1) as a function of temperature for the 147 cm^{-1} mode to extract the activation energy E_a for this mode according to Equation 2.32.

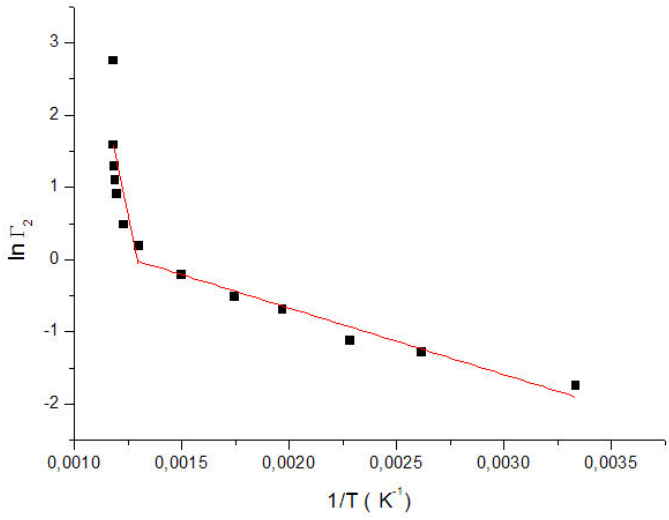

Figure 3.15: The damping constant (Γ_2) as a function of temperature for the 147 cm^{-1} mode to extract the activation energy E_a for this mode according to Equation 2.32.

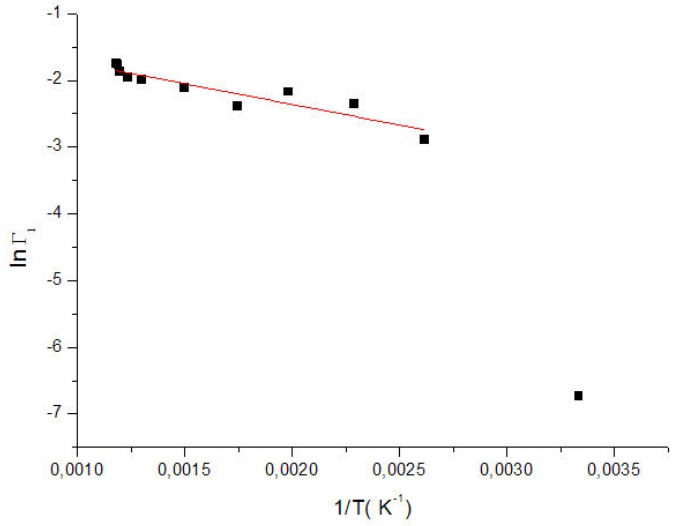

Figure 3.16: The damping constant (Γ_1) as a function of temperature for the 207 cm^{-1} mode to extract the activation energy E_a for this mode according to Equation 2.32.

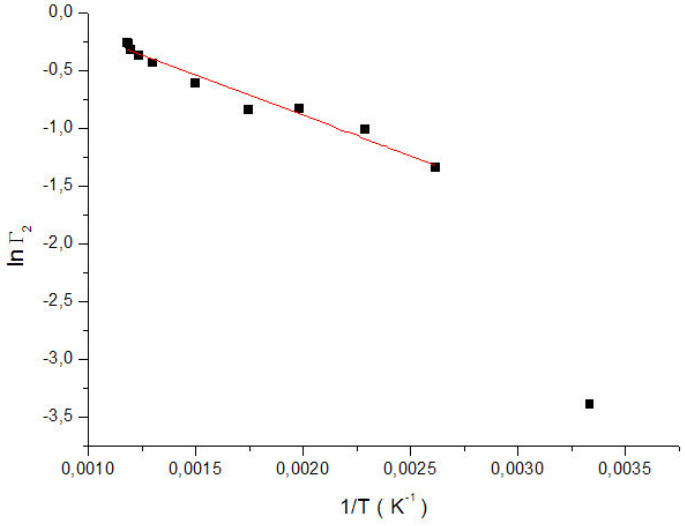

Figure 3.17: The damping constant (Γ_2) as a function of temperature for the 207 cm^{-1} mode to extract the activation energy E_a for this mode according to Equation 2.32.

3.5 Calculation of the Grüneisen Parameter and the Raman Frequency for the 207 cm^{-1} Mode

From the study of Tucker *et al.* [37] on $\alpha - \beta$ phase transition, we made use of the volume dependence of the unit cell varying with the temperature, as shown in Figure 2.16. For simplicity, we assigned subscripts "s" and "c" to the volume and frequency which refer to the solid squares and solid circles in Figure 2.16, respectively. Firstly, we fitted the temperature dependent unit cell volume to a quadratic formula according to the Equation 2.43 for both data. Then using Equation 2.44, we also fitted for the 207 cm^{-1} mode frequency. We plot in Figure 3.18 the data fitted with the relevant coefficients, as given in Table 3.4

Table 3.4: Calculations of coefficients from the fitted volume data for squares and circles, V_s and V_c

Volume	a_0	a_1 (10^{-4})	a_2 (10^{-6})	**Temperature interval (K)**
V_c	112.2	-3.5	7.1	$6.6 < T < 854.6$
V_s	112.3	10	8.0	$6.6 < T < 855.9$

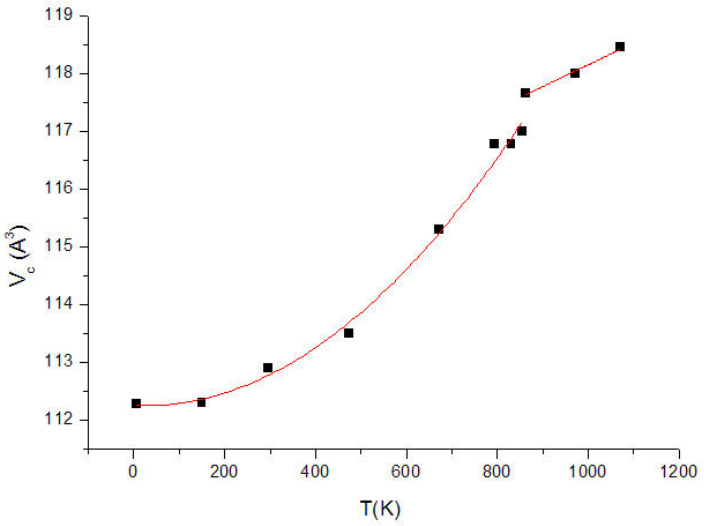

Figure 3.18: Temperature dependence of the unit cell volume for solid circles in Figure 2.16

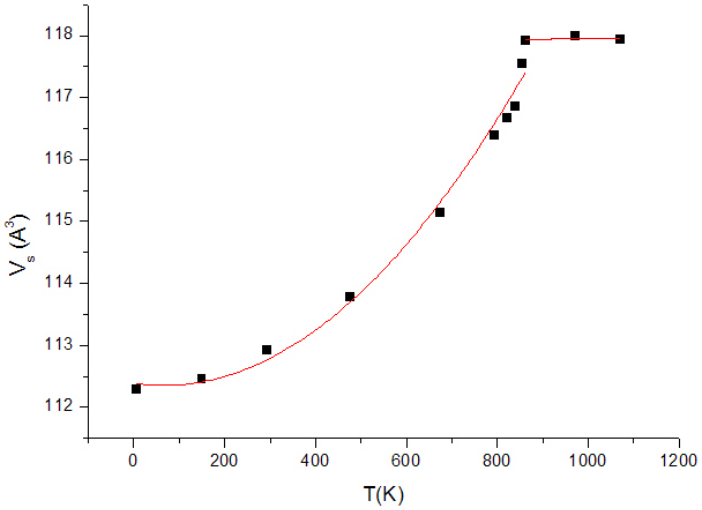

Figure 3.19: Temperature dependence of the unit cell volume for solid squares in Figure 2.16

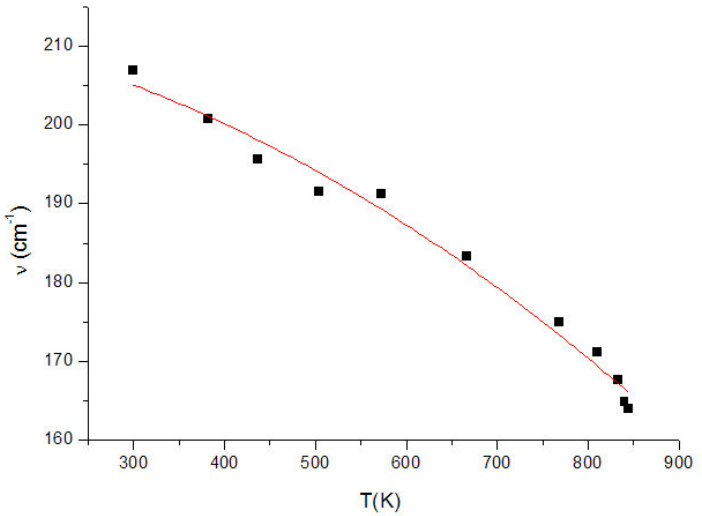

Figure 3.20: Temperature dependence of the Raman frequency for the 207 cm^{-1} mode.

Table 3.5: Values of the coefficients obtained for the 207 cm^{-1} mode frequency according to Equation 2.44.

Raman mode (cm^{-1})	b_0	b_1 (10^{-3})	b_2 (10^{-5})	**Temperature interval (K)**
207	213.6	-13	-5.0	$299.8 < T < 844.7$

Table 3.6: Values of the coefficients obtained as the frequency difference for the 207 cm^{-1} (Figure 3.21)

Frequency shift	c_0	c_1 (10^{-3})	c_2 (10^{-5})	**Temperature interval (K)**
$\Delta\nu_s$	510	-2.0	3.3	$299.8 < T < 844.7$

Table 3.7: Values of the coefficients obtained as the frequency difference for the 207 cm^{-1} (Figure 3.22)

Frequency shift	d_0	d_1 (10^{-3})	d_2 (10^{-6})	**Temperature interval (K)**
$\Delta\nu_c$	4.94	-4.0	5.2	$299.8 < T < 844.7$

Table 3.8: Values of the mode Grüneisen parameter γ_p determined by using the neutron diffraction data (Figure 3.18) and the unit-cell volume of the average structure of quartz (Figure 3.19) with the values of the volume and the Raman frequency at T=0 K.

V (A^3)	γ_p	V_0 (A^3)	ν_1 (cm^{-1})
V_c	5.5	112.2	213.6
V_s	2.5	112.3	213.6

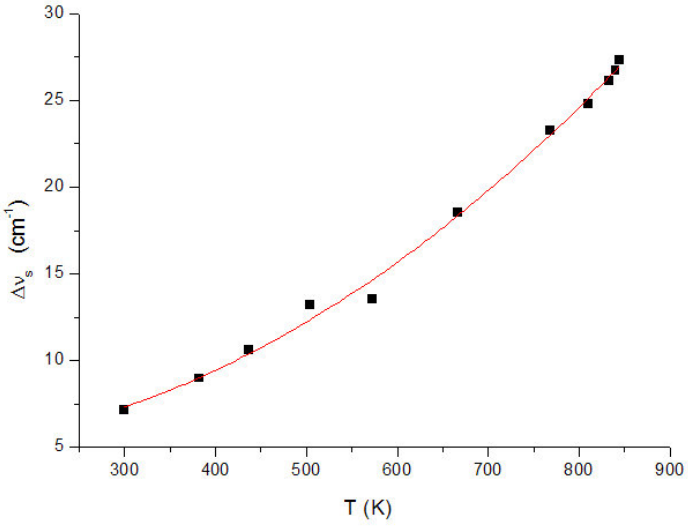

Figure 3.21: The frequency difference for the 207 cm^{-1} Raman mode.

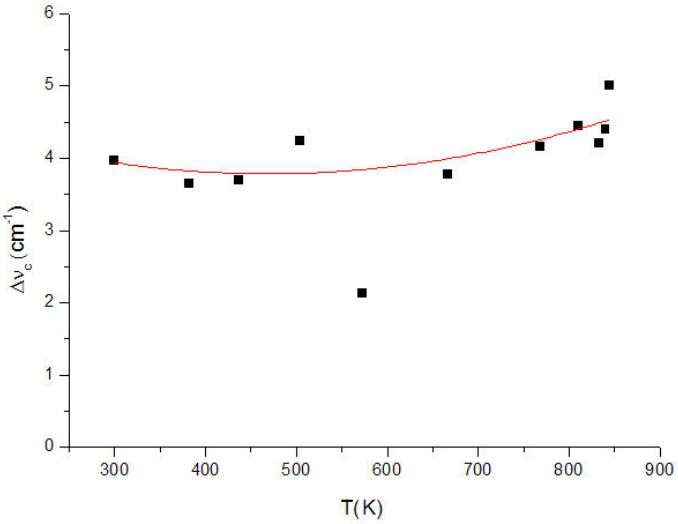

Figure 3.22: The frequency difference for the 207 cm^{-1} Raman mode.

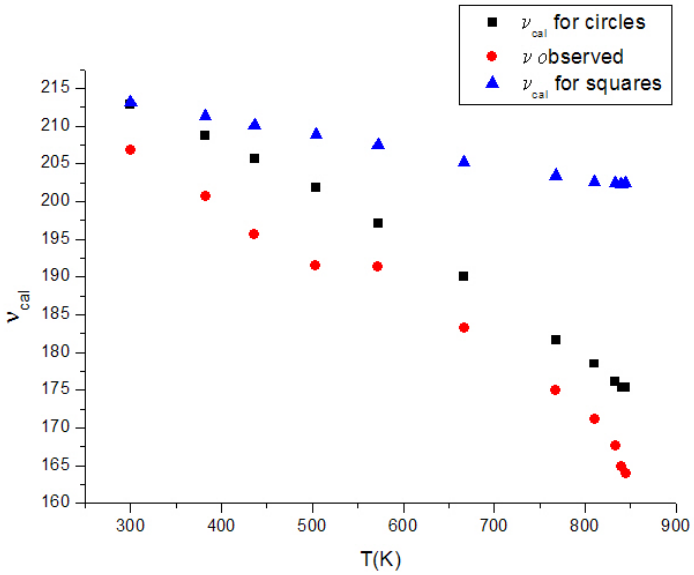

Figure 3.23: The comparison for the 207 cm^{-1} Raman mode calculated frequencies according to Equation 2.42 with the observed data.

CHAPTER 4

DISCUSSIONS AND COMMENTS

The observed Raman frequencies for the lattice modes of 147 and 207 cm^{-1} were related to the order parameter (polarization) for the $\alpha - \beta$ transition (T_c = 846 K) in quartz, as shown in Figures 3.10 and 3.11, respectively. Since the Raman frequency of the weak mode of symmetry A_1 (147 cm^{-1}) goes to zero when approaching the $\alpha - \beta$ transition temperature T_c as observed experimentally [3], this mode exhibits a soft mode behavior according to $\nu^2 = k \mid T - T_c \mid^{\beta}$ within the framework of the soft mode theory [45]. This leads to the $\alpha - \beta$ transition in quartz as a second order transition, which was also considered by Ginzburg [39] within the Landau′s phenomenological theory. However, our analysis of the ν^2 vs. $T - T_c$ gives rise to the value of $\beta = 0.5$, as also obtained previously [3] within the temperature interval of $4.3 <\mid T - T_c(K) \mid< 546.3$ according to our analysis given here. This is not in agreement with the value of $\beta = 1/2$ from the ν vs. $T - T_c$ or $\beta = 1$ from the ν^2 *vs.* $T - T_c$ data according to the soft mode theory, as also pointed out previously [3]. So, the square of the Raman frequency (ν^2) of the lattice modes of 147 cm^{-1} and 207 cm^{-1} correlates with the order parameter (polarization P) linearly, as shown in Figures 3.10 and 3.11, respectively for the $\alpha - \beta$ transition in quartz. Within the temperature interval of $0.5 < T - T_c(K) < 4.3$ which is close to the $\alpha - \beta$ transition in quartz, our analysis of the ν^2 vs. $T - T_c$ for the 147 cm^{-1} mode gives the value of $\beta = 1.2$. This exponent value is close to the $\beta = 1$ predicted from the soft mode theory. This indicates that the A_1 (147 cm^{-1}) exhibits a soft mode behavior within the temperature interval of about 4 K just below T_c for the $\alpha - \beta$ transition in quartz.

Regarding the temperature dependence of the Raman bandwidths of the 147 cm^{-1} mode, the Γ values calculated from Equations 2.25 and 2.26 (Figures 3.3 and 3.5) behave differently from those calculated for the 207 cm^{-1} mode (Figures 3.7 and 3.8). The Γ values calculated

from Equation 2.25 for the 147 cm^{-1}mode (Figure 3.3) is lower than those calculated from Equation 2.26 (Figure 3.5). Also, the Γ values calculated from Equation 2.25 (Figure 3.7) are much lower than those calculated using Equation 2.26 (Figure 3.8) for the 207 cm^{-1} mode within a large temperature region below T_c down to $T - T_c = -500K$.

Considering the critical behavior of the damping constant or the bandwidths varying with the temperature below T_c, our Γ values calculated from Equations 2.25 and 2.26 show the expected behavior for the Raman mode of 147 cm^{-1} (Figures 3.3 and 3.5). As predicted from the soft mode theory ($\nu \rightarrow 0 \; as \; T \rightarrow T_c$), the bandwidth Γ of the 147 cm^{-1} Raman mode (Figures 3.3 and 3.5) diverges or goes to infinity as a soft mode when the $\alpha - \beta$ transition is approached from the low temperatures ($\alpha - phase$) and it goes to zero well below T_c (about $T - T_c = -400K$). Our exponent values of $\beta \approx 0.2$ (Equation 2.25) and ≈ 0.3 (Equation 2.26) which were deduced from the power-law analysis (Equation 2.29) for the 147 cm^{-1} Raman mode as given in Table 3.2, can be compared with the value of $\beta = 0.5$ from the ν^2 vs. T data ($\nu^2 = k \mid T - T_c \mid^{\beta}$) and also with the value of $\beta = 0.2$ deduced from the analysis of the 207 cm^{-1} Raman mode within the same temperature interval (Table 3.1). This indicates that the critical behavior of the soft mode (147 cm^{-1}) can be described consistently by the critical exponent for the order parameter as obtained from the temperature dependence of the Raman frequency ($\nu^2 = k \mid T - T_c \mid^{\beta}$) and that dependence of the bandwidth (Equation 2.29) for this mode. This critical behavior is not seen for the 207 cm^{-1} mode, as observed experimentally [3] and also from our calculated bandwidths (Figures. 3.7 and 3.8). So, the mechanism of the $\alpha - \beta$ transition and the soft mode behavior is attributed to the 147 cm^{-1} Raman mode of quartz. In regard to the values of the activation energy which we extracted from Equation 2.32 by using our calculated values of the bandwidth for the 147 cm^{-1} and 207 cm^{-1} modes (Equations 2.25 and 2.26), they are comparable with the value of $k_BT = 0.072$ eV for the $\alpha - \beta$ transition in quartz. As given in Table 3.3, for the soft mode of the 147 cm^{-1} the E_a values increase from ~0.1 eV to about 1.3 eV as approaching the transition temperature T_c on the basis of both soft mode-hard mode coupling model (Equation 2.25) and the energy fluctuation model (Equation 2.26). In particular, our extracted value of $E_a = 0.07$ eV within the temperature interval of $299.8 < T(K) < 769.8$ for the 147 cm^{-1} mode (Table 3.3) is the same as the k_BT_c value for the $\alpha - \beta$ transition in quartz. For the 207 cm^{-1} Raman mode , our E_a value of 0.005 eV for all the temperature range below the T_c (Table 3.3) is too small to be compared with the k_BT_c value for the $\alpha - \beta$ transition in this crystal. This indicates

that the height of the barrier decreases much faster than the energy difference between the two minima in the α phase (ordered phase) leads to a double minimum configuration with random occupation of the SiO_4 atoms in the β phase (disordered phase) on the basis of the ad-hoc phenomenological model [3]. This suggests that the $\alpha - \beta$ transition in quartz is an order-disorder transition.

The temperature dependence of the Raman frequencies for the lattice modes was analyzed using the experimental data for the $\alpha - \beta$ transition in quartz. The Raman bandwidths of those modes were calculated as a function of temperature for the $\alpha - \beta$ transition in this crystal by using the soft mode hard mode coupling model and the energy fluctuation model.

Our results show that the calculated Raman bandwidths for the 147 cm^{-1} lattice mode (soft mode) increase largely as the $\alpha - \beta$ transition temperature is approached. This is in accordance with the soft mode behavior of the Raman frequency vanishing at $T = T_c$, as expected from the soft mode theory. Our calculated bandwidths of the Raman modes studied here, can be compared with the experimental measurements for the $\alpha - \beta$ transition in quartz when available in the literature.

The Raman frequency of the 207 cm^{-1} mode was calculated (Equation 2.42) using the volume data [14] through the Grüneisen parameter γ_p of this mode (Equation 2.39) for the $\alpha - \beta$ transition in quartz at various temperatures, as given in Figure 3.23. This is in accordance with the observed Raman frequencies [3] for the 207 cm^{-1} mode (Figure 3.20 or Figure 3.23) which decrease as the temperature increases towards the transition temperature T_c. Although this decrease in the Raman frequency with increasing temperature is exhibited for the 207 cm^{-1} mode, the absolute values of the Raman frequency ν are completely different except at T=300 K. Since the volume values were obtained using two different techniques [14], namely, the neutron diffraction (Figure 3.18) and the unit-cell volume of the average structure of quartz (Figure 3.19), we deduced two γ_p values for the 207 cm^{-1} Raman mode (Table 3.8). Thus, the two sets of the Raman frequency of this mode were calculated with the γ_p values according to Equation 2.42, as plotted in Figure 3.23. It is clear from this figure that the Raman frequencies calculated using (the symbol solid square) the neutron diffraction data (Figure 3.18) follow closely the observed data [3]. This indicates that the value of the Grüneisen parameter for the 207 cm^{-1} is in fact γ_p =5.5 instead of 2.5 on the basis of our calculated Raman frequencies in comparison with the experimental data [10], as shown in

Figure 3.23. On the other hand, $\Delta\nu$ values of the Raman frequency shift for the 207 cm^{-1} mode, which were deduced from Equation 2.42 by using the two sets of volume data [14] show a different temperature dependence (Figures 3.21 and 3.22). For the volume data (Figure 3.19), $\Delta\nu$ increases as the temperature increases towards T_c (Figure 3.21) whereas $\Delta\nu$ values obtained by using the volume data (Figure 3.18) remains almost constant (around 4 cm^{-1}). We also note that the $\Delta\nu$ values (Figure 3.21) which were obtained from the volume data given in Figure 3.19, are much larger than those given in Figure 3.22. This also indicates that the smaller $\Delta\nu$ values (Figure 3.22) for the 207 cm^{-1} mode with the Grüneisen parameter of γ_p=5.5 represent the observed behavior of this lattice mode for the $\alpha - \beta$ transition in quartz. The frequency shift due to the atomic motions of this lattice mode can be associated with the $\alpha - \beta$ transition in quartz, as also pointed out previously [16]. It was reported many years ago that this lattice mode moves toward the Rayleigh line as the T_c is approached and that it disappears completely in the β phase [17]. However, it has been observed that the 207 cm^{-1} mode still exists above T_c as a broad band centered at 162 cm^{-1} [3]. With increasing temperature in the α phase, the Raman frequency of this phonon mode decreases, as observed experimentally (Figure 3.20), which causes the increasing disorder towards the β phase. It has been pointed out previously that the extensive disorder in the β phase is due to the excitation of the soft mode. So that, the low-energy high-amplitude vibrations contribute to the disorder in the β phase [14].

The Raman frequency of the lattice mode (207 cm^{-1}) was calculated as a function of temperature by using the volume data for the $\alpha - \beta$ transition in quartz. The calculation of the Raman frequency of this mode was performed by determining the mode Grüneisen parameter using the observed Raman data, which was kept constant throughout the $\alpha - \beta$ transition in this crystal. Our calculated frequencies which were obtained by using the neutron diffraction data, predict the observed Raman frequencies of this lattice mode for the $\alpha - \beta$ transition in quartz. However, our frequencies calculated from the unit-cell volume of the average structure of quartz, are in disagreement with the observed Raman data.

It is shown here that our method of calculating the Raman frequencies from the neutron scattering volume data is better match for explaining the experimental data with respect to the unit-cell volume average for the $\alpha - \beta$ transition in quartz.

REFERENCES

[1] J.F. Scott. Soft-mode spectroscopy: Experimental studies of structural phase transitions. *Review of Modern Physics*, 46(1):83–128, January 1974.

[2] Y.Yu. Peter and M. Cardona. *Fundamentals of Semiconductors*. Springer Press, Berkeley, USA and Stuttgart, Germany, fourth edition, March 2010.

[3] S.M. Shapiro, D.C. O'Shea, and H.Z. Cummins. Raman scattering study of the alpha-beta phase transition in quartz. *Physical Review Letters*, 19(7):361, August 1967.

[4] G. Dolino, J.P. Bachhneimer, and C.M.E. Zeyen. Observation of an intermediate phase near the $\alpha-\beta$ transition of quartz by heat capacity and neutron scattering measurements. *Solid State Communications*, 45:295, 1983.

[5] H. Yao and I. Hatta. Phase transitions of quartz studied by a.c. calorimetry. *Thermochimica Acta*, 266:301, November 1995.

[6] K. Gouhara, Y.H. Li, and N. Kato. Studies on the $\alpha-\beta$ transition of quartz by means of in situ x-ray topography. *Journal of the Physical Society of Japan*, 52:3821, 1983.

[7] K. Gouhara, Y.H. Li, and N. Kato. Observation of satellite reflections in the intermediate phase of quartz. *Journal of the Physical Society of Japan*, 52:3697, 1983.

[8] K. Gouhara and N. Kato. Refined observations of satellite reflections in the intermediate phase of quartz. *Journal of the Physical Society of Japan*, 53:2177, 1984.

[9] M. Midorikawa, K. Gouhara, and Y. Ishibashi. Dilatometric and dielectric studies of an incommensurate transition in quartz. *Journal of the Physical Society of Japan*, 53(8):2431, August 1984.

[10] J.P. Bachheimer. An anomaly in the β phase near the $\alpha-\beta$ transition of quartz. *Journal of Physical Letters*, 41:L 559, 1980.

[11] G. Dolino, J.P. Bachheimer, F. Gervais, and A.F. Wright. La transition alpha -beta du quartz: le point sur quelques problemes actuels: transition ordre-desordre ou displacive, comportement thermodynamique. *Bulletin de Mineralogie*, 106(3):267, 1983.

[12] Pine A.S.G. and P.E. Tannenwald. Temperature dependence of Raman linewidth and shift in $\alpha-$quartz. *Physical Review Letters*, 178:1424, February 1969.

[13] T. Shigenari, Y. Limura, and Y. Takagi. On the static nature of the opalescence near the $\alpha-\beta$ transition in a quartz crystal. *Optics Communications*, 31(1):57, October 1979.

[14] M.G. Tucker, D.A. Keen, and M.T. Dove. A detailed structural characterization of quartz on heating through the $\alpha-\beta$ phase transition. *Mineralogical Magazine*, 65:489, 2001.

[15] M.G. Tucker, M.T. Dove, and D.A. Keen. Simultaneous analyses of changes in long-range and short-range structural order at the displacive phase transition in quartz. *Journal of Physics: Condensed Matter*, 12:L 723, 2000.

[16] D.A. Kleinman and W.G Spitzer. Theory of the optical properties of quartz in the infrared. *Physical Review Letter*, 125(1):16, January 1962.

[17] P.K. Narayanaswamy. The alfa-beta transformation in quartz. *Proceedings of the Indian Academy of Sciences*, A28:417, 1948.

[18] A.J. Hughes and A.W. Lawson. Cylindrical approximation and the $\alpha - \beta$ quartz transition. *Journal of Chemical Physics*, 36:2098, 1962.

[19] M. Matsuura, H. Yao, K. Gouhara, I. Hatta, and N. Kato. Heat capacity in the $\alpha - \beta$ phase transition of quartz. *Journal of the Physical Society of Japan*, 54:625, February 1985.

[20] N.N. Sinel'nikov. *Doklady Akademii Nauk SSSR*, 92:369, 1953.

[21] M. Mosbah, J.P. Duraud, and R. Clucchiatti. Use of the $\alpha - \beta$ quartz transition to momnitor the temperature increase produced by a proton microbeam. *Nuclear Instruments and Methods in Physics Research B*, 130:171, 1997.

[22] M.T. Dove. *Introduction to Lattice Dynamics*. Cambridge University Press, Great Britain, 1993.

[23] I. Van der Molen. The shift of the $\alpha - \beta$ transition temperature of quartz associated with the thermal expansion of granite at high pressure. 73:323, March 1981.

[24] E. Philippot, A. Goiffon, A. Ibanez, and M. Pintard. Structure deformations and existence of the $\alpha - \beta$ transition in MXO_4 quartz like materials. 110:356, 1994.

[25] L.Sh. Bazarov, T.N. Drebushchak, V.I. Gordeeva, and F.Kh. Urakaev. Character of change in the work of nucleation of β-quartz, diamond and aluminum hydrite ($\alpha - AlH_3$) crystals in homogeneous media. 206:75, June 1999.

[26] M.A.T.M. Broekmans. Structural properties of quartz and their potential role for asr. 53:129, 2004.

[27] C. Hammond. *The Basics of Crystallography and Diffraction*. Oxford University Press, USA, third edition, 2009.

[28] Stephen J. Blundell and Katherine M. Blundell. *Concepts in Thermal Physics*. Oxford University Press, Great Britain, 2006.

[29] C. Kittel. *Introduction to Solid State Physics*. John Wiley and Sons, Inc., Canada, seventh edition, 1996.

[30] A.B. Pippard. *The Elements of Classical Thermodynamics*. Cambridge University Press, London, 1966.

[31] Arthur R. Von Hippel. *Dielectric Materials and Applications*. The M.I.T Press, Massachusetts, 1961.

[32] R. Blinc and E. Zeks. *Soft Modes in Ferroelectrics and Antiferroelectrics*. American Elsevier, New York, 1974.

[33] B.A. Strukov and A.P. Levanyuk. *Ferroelectric Phenomena in Crystals*. Springer, Germany, 1998.

[34] J.J. Quinn and K. Yi. *Solid State Physics Principles and Modern Applications*. Springer, New York, 2010.

[35] I. Sunagawa. *Crystals Growth, Morphology and Perfection*. Cambridge University Press, USA, 2005.

[36] W. Heywang, K. Lubitz, and W. Wersing. *Piezoelectricity*. Springer, Germany, 2008.

[37] M.G. Tucker, D.A. Keen, and M.T. Dove. A detailed structural characterization of quartz on heating through the α–β phase transition. *Mineralogical Magazine*, 65(4):489, August 1962.

[38] W. Cochran. Crystal stability and the theory of ferroelectricity. *Physical Review Letter*, 3(9):412, November 1959.

[39] V.L. Ginzburg. The scattering of light near points of phase transition in solids. *Soviet Physics Uspekhi*, 5(4):649, January-February 1963.

[40] I. Laulicht and N. Lucknar. Internal-mode line broadening by proton jumps in KH_2PO_4. *Chemical Physics Letter*, 47(2):237, November 1977.

[41] Y. Yamada, M. Mori, and Y. Noda. A microscopic theory on the phase transition in NH_4B_r-an Ising spin phonon coupled system. *Journal of the Physical Society of Japan*, 32:1565, 1972.

[42] M. Matsushita. Anomalous temperature dependence of the frequency and damping constant of phonons near T_λ in ammonium halides. 65:23, 1976.

[43] I. Laulicht. On the drastic temperature broadening of hard mode Raman lines of ferroelectric KDP type crystals near T_c. *Journal of Physics and Chemistry of Solids*, 39(8):901, 1978.

[44] D.L. Huber, D. Laura-Ccahuana, M. Tovar, and M.T. Causa. Electron spin resonance linewidth, susceptibility and conductivity in doped manganites. *Journal of Magnetism and Magnetic Materials*, 130(2):604, 2007.

[45] W. Cochran. Crystal stability and the theory of ferroelectricity part ii. piezoelectric crystals. *Advances in Physics*, 10(40):401, 1961.